Cerebral Cortex, March 2021;31: 1807–1826

doi: 10.1093/cercor/bhaa333
Advance Access Publication Date: 18 November 2020
Original Article

ORIGINAL ARTICLE

Pathways for Contextual Memory: The Primate Hippocampal Pathway to Anterior Cingulate Cortex

Jingyi Wang[1], Yohan John[1] and Helen Barbas[1,2]

[1]Department of Health Sciences, Neural Systems Laboratory, Boston University, Boston, MA 02215, USA and [2]Graduate Program in Neuroscience, Boston University and School of Medicine, Boston, MA 02215, USA

Address correspondence to Helen Barbas, Boston University, 635 Commonwealth Ave., Room 431, Boston, MA 02215, USA. Email: barbas@bu.edu.

Abstract

The anterior cingulate cortex (ACC) is one of the few prefrontal areas that receives robust direct hippocampal terminations. This pathway may enable current context and past experience to influence goal-directed actions and emotional regulation by prefrontal cortices. We investigated the still ill-understood organization of the pathway from anterior hippocampus to ACC (A24a, A25, A32) to identify laminar termination patterns and their postsynaptic excitatory and inhibitory targets from system to synapse in rhesus monkeys. The densest hippocampal terminations targeted posterior A25, a region that is involved in affective and autonomic regulation. Hippocampal terminations innervated mostly excitatory neurons (~90%), suggesting strong excitatory effects. Among the smaller fraction of inhibitory targets, hippocampal terminations in A25 preferentially innervated calretinin neurons, a pattern that differs markedly from rodents. Further, hippocampal terminations innervated spines with D1 receptors, particularly in the deep layers of A25, where D1 receptors are enriched in comparison with the upper layers. The proximity of hippocampal terminations to D1 receptors may enable dopamine to enhance information transfer from the hippocampus to A25 and contribute to dopaminergic influence downstream on goal-directed action and emotional control by prefrontal cortices, in processes that may be disrupted by excessive dopamine release during uncontrollable stress.

Key words: anterior cingulate cortex, contextual memory, dopamine, hippocampus, inhibitory neurons

Introduction

The strongest unidirectional pathway from hippocampus to the prefrontal cortex in primates is directed to anterior cingulate cortex (ACC; Barbas and Blatt 1995; Insausti and Munoz 2001; Aggleton et al. 2015), reviewed in (Insausti et al. 2017). This pathway is analogous to the hippocampal-medial prefrontal pathway in rodents (Jay and Witter 1991; Jay et al. 1992; Verwer et al. 1997; Thierry et al. 2000), reviewed in (Alexander et al. 2019a). Studies in rodents have revealed critical roles for this pathway in decision-making, goal-directed behavior, working memory, and emotion regulation, and some of these functions have also been described in primates (Wallis et al. 2019; Zeredo et al. 2019), reviewed in (Godsil et al. 2013; Eichenbaum 2017; Alexander et al. 2019a; Bachevalier 2019). Disruption of the hippocampal pathway to ACC has been implicated in psychiatric diseases in humans including depression, post-traumatic stress disorder (PTSD), and schizophrenia (Seminowicz et al. 2004; Admon et al. 2009; Milad et al. 2009; Qiu et al. 2010; Dickie et al. 2011; Goveas et al. 2011; Koch et al. 2013).

Extensive studies in rats have shown that the hippocampal pathway originates in the temporal two thirds of CA1 and the subiculum and terminates robustly in specific layers of infralimbic (IL) and prelimbic (PL) regions of the medial prefrontal cortices (mPFC) (Jay and Witter 1991; Jay et al. 1992; Verwer et al. 1997; Thierry et al. 2000). The analogous primate pathway, from hippocampus to ACC, has not yet been studied in detail (Barbas and Blatt 1995; Insausti and Munoz 2001; Aggleton et al. 2015), reviewed in (Insausti et al. 2017). Moreover, because the primate prefrontal cortex is a larger and more differentiated region than in rodents, there is no consensus regarding analogy between mPFC in rodents and ACC in primates (Godsil et al. 2013; Vogt et al. 2013; Alexander et al. 2019a). In this context, our first

goal was to investigate the topographic distribution of the hippocampal pathway in ACC in rhesus monkeys qualitatively and quantitatively, to enable comparison with the rodent literature.

In rats, the hippocampal terminations primarily contact excitatory neurons in mPFC (Jay et al. 1992). In addition, a small but significant number of hippocampal terminals interact with inhibitory neurons, targeting preferentially parvalbumin (PV) inhibitory neurons (Gabbott et al. 2002; Tierney et al. 2004; Parent et al. 2010), which exercise strong perisomatic inhibition on nearby cortical pyramidal neurons (DeFelipe 1997). Corresponding information on hippocampal input to inhibitory neurons in primate ACC is lacking. To fill this gap, our second goal was to investigate the excitatory and inhibitory postsynaptic targets of the hippocampal terminations in ACC, as well as the presynaptic hippocampal features from the system to the synapse. We used confocal microscopy and serial electron microscopy (EM) sections to visualize hippocampal terminations and their postsynaptic sites. To identify different neurochemical groups of inhibitory neurons in primates, we stained for the calcium-binding proteins, calretinin (CR), calbindin (CB), and PV, which label neurochemical and functionally distinct classes of inhibitory neurons and also show preferential laminar distribution in primates (Conde et al. 1994; Gabbott and Bacon 1996a, 1996b; DeFelipe 1997; Gabbott et al. 1997; Meskenaite 1997; Wang et al. 2004; Melchitzky et al. 2005; Melchitzky and Lewis 2008; Rocco et al. 2016).

An additional question is whether the hippocampal input to prefrontal areas may be modulated by dopaminergic signaling, known to have powerful effects on prefrontal cortex (reviewed in Williams and Goldman-Rakic 1995; Seamans and Yang 2004; Arnsten et al. 2015). Dopaminergic D1 receptors are abundant in prefrontal cortices, and especially the mPFC of rats and ACC of primates (Vincent et al. 1993; Smiley et al. 1994; Palomero-Gallagher et al. 2009). In rat mPFC, hippocampal and dopaminergic terminations are located near each other (Carr and Sesack 1996), and long-term potentiation can be enhanced through activation of the ventral tegmental area (VTA) terminations or by applying D1 receptor agonists (Gurden et al. 1999). We thus sought to determine if similar dopaminergic influence may occur in the primate hippocampus-to-ACC pathway. To address this issue, our third goal was to investigate the relationship between hippocampal terminations and postsynaptic D1 receptors in A25.

Our multilevel analyses included the primate ACC (A32, A24, and A25). Our findings revealed that hippocampal terminations preferentially targeted mid-to-posterior A25 in the ACC. Within A25, hippocampal terminations predominantly innervated excitatory neurons, with a small proportion terminating on CR or CB inhibitory neurons. Moreover, the relationship between hippocampal terminations and D1 receptors was different in the upper and deep layers of A25. These findings suggest a predominant excitatory role of hippocampal inputs in ACC, which may be modulated by dopamine in health and disease.

Materials and Methods

Experimental Design

To study the distribution and postsynaptic targets of hippocampal terminations in ACC, we injected anterograde fluorescent tracers in the anterior hippocampus at the level of the uncus, known to issue most projections to ACC (Barbas and Blatt 1995). We employed immunohistochemistry to label hippocampal terminations, different classes of inhibitory neurons and D1 receptors in ACC. We investigated the hippocampal terminations from the system to synapse using light microscopy, confocal microcopy, and EM.

Briefly, our study can be divided into three parts, as shown in Figure 1A: (1) topographic distribution of the hippocampal terminations in ACC (Fig. 1A(*a*)); (2) features of the presynaptic elements and excitatory or inhibitory postsynaptic targets of the hippocampal terminations in ACC (Fig. 1A(*b*)); (3) interaction between hippocampal terminations and D1 receptor in the upper and deep layers of A25 (Fig. 1A(*c*)).

In the first part, we focused on A25, A32, and A24a of ACC, which receive robust unidirectional pathways from the hippocampus in monkeys (Aggleton et al. 2015). To map the hippocampal terminations in ACC, we used an antibody to each fluorescent tracer and processed series of coronal sections through ACC using diaminobenzidine (DAB). The brown precipitate of DAB on hippocampal terminations allowed us to visualize the pathway using bright-field microscopy. We then counterstained this series of tissue with Nissl, which helped to delineate areas and layers of ACC using cytoarchitecture. With this series of sections through ACC, we used a semiautomated system (StereoInvestigator) to map hippocampal axons qualitatively and used unbiased stereology to study the distribution of hippocampal terminations in ACC quantitatively.

The goal of the second part was to study the features of presynaptic and postsynaptic sites from the anterior hippocampus to the ACC. We first immunostained fluorescent tracers to view hippocampal terminations using DAB in coronal sections through ACC, as in the first part (above). This process allowed us to study the size of hippocampal axon boutons in A25, A32, and A24 using light microscopy. We then focused on A25, the major target of hippocampus in ACC to study features of its postsynaptic targets using confocal microscopy and EM. In the same coronal sections, we employed double-labeling immunohistochemistry using an antibody against the fluorescent tracer and an antibody against one of the calcium-binding proteins using distinct colors; this made it possible to view the hippocampal pathway and inhibitory postsynaptic sites simultaneously. We exhaustively examined all hippocampal boutons in stacks of images using confocal microscopy, and analyzed sites of apposition between hippocampal boutons and inhibitory postsynaptic sites.

To study the hippocampal pathway and one or two distinct postsynaptic sites labeled for markers of inhibitory neurons in the EM, we labeled the pathway with DAB and one or two calcium-binding proteins using gold or TMB on the same coronal sections through A25; we then processed the double or triple-labeled sections to view in the EM. High-resolution EM allowed us to analyze the morphologic features of hippocampal terminations and excitatory and inhibitory postsynaptic sites.

In the third part, we first investigated the distribution of D1 receptors in the upper and deep layers of A25 by applying immunohistochemistry to label D1 receptors in A25 using fluorescence for confocal microscopy. In two animals, we double labeled D1 receptors (using TMB) and hippocampal terminations (using DAB) in the same tissue sections through A25. We then processed the tissue for EM. These procedures allowed us to investigate the relationship between D1 receptors and hippocampal terminations in A25 at the synaptic level.

We used two-tailed *t* test for paired comparisons and ANOVA with Bonferroni's post hoc test for multiple comparisons, and

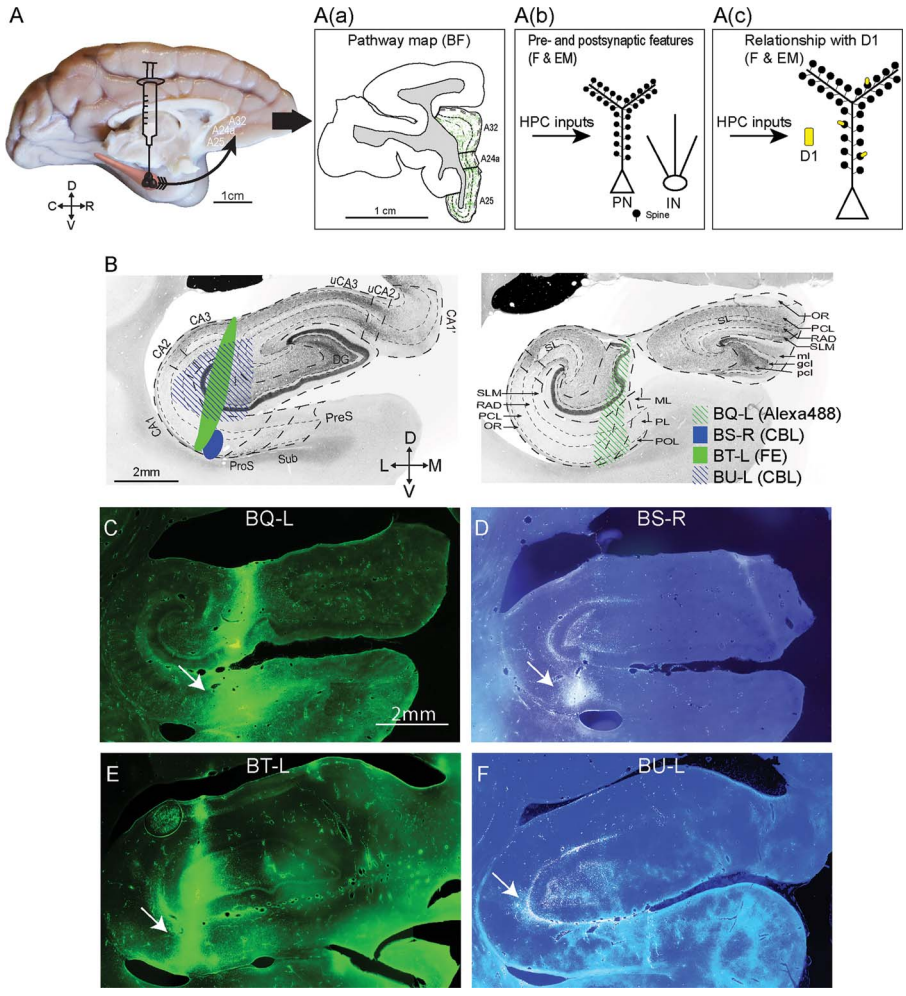

Figure 1. Experimental design and injection sites in the hippocampus. (*A*) Scheme of the anterograde fluorescent tracer trajectory: from projection neurons at the injection site (black cones) in the hippocampus along the axons to the ACC; the arrow shows the pathway direction. *A*(*a*) Immunohistochemistry: Mapping the hippocampal pathway terminations from coronal ACC sections with an antibody to each fluorescent tracer and processing tissue sections using DAB to visualize the pathway with brightfield microscopy (goal 1). *A*(*b*) Two methods were used to study presynaptic features and postsynaptic targets on distinct types of inhibitory neurons of hippocampal terminations: 1, Immunofluorescence: coronal sections through ACC showing the fluorescent labeled pathway from the hippocampal injection site were processed with an antibody against one of the calcium-binding proteins to study appositions of labeled hippocampal axonal boutons that made close contact with inhibitory postsynaptic sites using fluorescence microscopy; 2, Immunohistochemistry: double or triple immunohistochemistry was performed (as in *A*(*a*)) to view hippocampal axonal boutons in ACC using DAB, as well as for one or two calcium-binding proteins to label inhibitory postsynaptic sites using gold labeling or TMB to distinguish the labels for EM viewing. This tissue was used to study morphological features of hippocampal synapses and their postsynaptic targets (goal 2). *A*(*c*) Immunofluorescence: Study of the distribution of D1 receptors in A25 using an antibody against D1 receptors alone. Immunohistochemistry: The procedure described in *A*(*b*) was used to label hippocampal terminations using DAB and D1 receptors using TMB to visualize them simultaneously in EM to investigate their relationship (goal 3). Abbreviations: BF: brightfield microscopy. F: fluorescence. EM: electron microscopy. PN: pyramidal neuron. IN: inhibitory neuron. (*B*) Photomicrographs of coronal sections of the hippocampus stained for acetylcholinesterase show the subregions (left) and layers (right) (adapted from Wang and Barbas 2018). The representative sections were selected to match the level of the injection site in each case. Left panel: anterior level through hippocampus shows subregions (marked by thick dotted lines). Right panel: posterior level through hippocampus shows layers (marked by thin dotted lines). The shades indicate the location of the injection sites for each case. Abbreviations of tracers: CBL, cascade blue; FE, fluoroemerald. (*C*–*F*) Fluorescent photomicrographs show the injection sites in the hippocampus. The arrows in *C*–*F* point to the injection sites. Scale bars: A, 1 cm; *B*–*F*: 2 mm. C, caudal; D, dorsal; L, lateral; M, medial; R, rostral; V, ventral. Abbreviation of the subregions (*B*, left): DG, dentate gyrus; CA, cornu ammonis; uCA2, uncal CA2; uCA3, uncal CA3; ProS, prosubiculum; Sub, subiculum; PreS, presubiculum. Abbreviation of the layers (*B*, right): SLM, stratum lacunosum moleculare; RAD, stratum radiatum; PCL, stratum pyramidale; OR, stratum oriens; SL, stratum lucidum; ml, molecular layer; gcl, granule cell layer; pcl, polymorphic cell layer; ML, molecular layer; PL, pyramidal cell layer; POL, polymorphic cell layer.

linear regression to test the relationship between postsynaptic density (PSD) surface area and bouton volume or diameter.

Surgery, Tracer Injections, and Perfusion

We studied pathways to ACC after injecting tracers in the hippocampus of rhesus monkeys (*Macaca mulatta*; $n = 4$; 3 females, Table 1). To study the D1 receptor distribution, we used two additional monkeys (Table 1). Experiments were conducted following protocols approved by the Institutional Animal Care and Use Committees at New England Primate Research Center, Harvard Medical School, and Boston University in accordance with National Institutes of Health (NIH) guidelines (Department of Health, Education, and Welfare Publication no. [NIH] 80-22, revised 1996, Office of Science and Health Reports, Division of Receipt and Referral/NIH, Bethesda, MD).

Table 1 Cases, tracers, injection sites, and analyses

Case	Sex	Age (years)	Hemisphere	Injection site	Tracer	Analysis		
						BF and F	EM	D1
BQ	Female	3.5	Left	Dentate gyrus, CA1, prosubiculum	Alexa488	AT, S, BS, A	MF, P	D1(EM)
BS	Female	3.5	right	CA1	CBL	S, BS,		
BT	Female	4	left	Dentate gyrus, CA1, CA3	FE	AT, S, BS, A	MF, P	D1(EM), D1 (F)
BU	Male	4	left	Dentate gyrus, CA3, CA2, CA1	CBL	S, BS,	MF	
BH	Female	3	Left	NA	NA	NA	NA	D1 (F)
BI	Female	3	Right	NA	NA	NA	NA	D1 (F)

Notes: BF, Bright-field microscopy; F, fluorescent microscopy; D1 (F), D1 receptor analyses for fluorescent microscopy; D1 (EM), D1 receptor analyses for EM analyses; A, appositions of presynaptic sites with confocal microscopy; AT, axon tracing; BS, bouton size analysis with bright-field microscopy; MF, morphological features using EM; P, postsynaptic targets identified with EM; S, stereology; NA, not applicable

Prior to surgery for injection of tracers, we conducted magnetic resonance imaging (MRI) to construct a map for precise targeting of hippocampal sites. For imaging, the monkeys were sedated with ketamine and then anesthetized with propofol and the head was placed in a stereotaxic apparatus (Kopf 1430M, David Kopf Instruments). After MRI, we calculated stereotaxic coordinates for the injection sites. About 1–3 weeks after imaging, the animals were sedated with ketamine followed by isoflurane to achieve a surgical level of anesthesia for injection of neural tracers under sterile procedures. The monkeys' head was fixed in the same stereotaxic apparatus and a small area of the cortex above the injection site was exposed. We used the coordinates calculated based on MRI to guide the insertion of microsyringes (5 or 10 µL syringes; Hamilton). Throughout surgery, we monitored vital signs, including the respiratory rate, oxygen saturation, heart rate, and temperature. We injected the anterior hippocampus with a mixture of retrograde (3 kDa) and anterograde (10 kDa) tracers (3–5 µL) with a final concentration of 10% (10 mg/mL in distilled water): Alexa Fluor488 (Invitrogen; case BQ); cascade blue (CBL; Invitrogen; case BS and BU), and fluoro-emerald (FE; Invitrogen; case BT), as shown in Figure 1.

After surgery, the monkeys recovered and rested for ~18 days to allow transport of tracers to destination in ACC. The animals then were perfused under an overdose of general anesthesia. For perfusion, the animals were first sedated with ketamine, and then given a lethal dose of anesthetic (sodium pentobarbital, to effect) and transcardially perfused with 4% paraformaldehyde and 0.2% glutaraldehyde in 0.1 M PBS. We then removed the brains from the skull and preserved them in ascending sucrose solutions at 4 °C for cryoprotection (10–25% sucrose in 0.01 m PBS, pH 7.4, with 0.05% sodium azide; Sigma-Aldrich). During sucrose infiltration, we removed the pia without disturbing the underlying brain structures. After a week, the brain sank in the final sucrose solution. We dried the brain surface and then froze it in isopentane solution (−70 °C; Thermo Fisher Scientific) and cut it on a freezing microtome ([AO Scientific Instruments] Reichert Technologies) in the coronal plane at 50 µm in 10 series. The free-floating sections were stored in −20 °C with antifreeze solution (30% ethylene glycol, 30% glycerol, and 0.05% sodium azide in 0.1 m PB, pH 7.4).

Acetylcholinesterase Staining

To identify the layers and subregions of the hippocampus, we used a histochemical procedure to stain sections through the hippocampus for acetylcholinesterase (AChE, Fig. 1B). Tissue sections were briefly rinsed with dH_2O (6×), incubated overnight at 4 °C in the AChE solution (0.2 mM ethopropazine hydrochloride [Sigma-Aldrich], 4 mM acetylthiocholine iodide [Sigma-Aldrich], 10 mM glycine [Thermo Fisher Scientific], 2 mM cupric sulfate pentahydrate [Thermo Fisher Scientific], and 50 mM sodium acetate [Sigma-Aldrich] in dH_2O [titrated to pH 5.0 with acetic acid]). Tissue sections then were rinsed with dH_2O (6×), incubated for 2–5 min at 25 °C in 8 mM sodium sulfide solution (sodium sulfide nonahydrate [Sigma-Aldrich], titrated to pH 7.8 with 3 N hydrochloric acid), rinsed with dH_2O (6×), followed by incubation for 5–30 min at 25 °C in 1% silver nitrate solution (Thermo Fisher Scientific). After final rinses in PBS (0.01 M, pH 7.4), we mounted tissue sections on gelatin-coated glass slides and coverslipped them with Entellan Mounting Medium.

Mapping Injection Sites Using Fluorescence Microscopy

To map the location of the injection sites, we mounted sections from one series that contained the tracer in the hippocampus on glass slides. Since the tracers were fluorescent, the injection sites could be viewed and captured directly using fluorescence microscopy (Fig. 1C–F; Model BX51, Olympus).

Tissue Processing To Visualize Hippocampal Terminations: Light Microscopy (Goal 1)

We used antibodies to each tracer in series of sections (1 in 20 sections) at the level of ACC and processed with DAB to visualize the hippocampal terminations. We counterstained every other section in the series with Nissl to study the cytoarchitecture. The immunohistochemistry procedure has been described previously (Wang and Barbas 2018). Briefly, free-floating sections went through PBS (0.01 M, pH 7.4) rinse, antigen retrieval (0.05 M sodium citrate) at 80 °C water bath for 30 min and glycine (0.05 M) incubation for 1 h. We then blocked the endogenous biotin- and avidin-binding sites with hydrogen peroxide (0.3%) incubation for 30 min and used the AB blocking solution (catalog #SP-2001, Vector Laboratories; RRID:AB_2336231) for another 30 min. To reduce nonspecific binding, we incubated the sections with preblocking solution for 1 h (10% normal goat serum [Vector Laboratories], 10% bovine serum albumin [BSA; Sigma-Aldrich], 0.2% BSA-c [Aurion], and 0.2% Triton X-100 [Sigma-Aldrich] in 0.01 m PBS) and incubated the sections with primary antibodies (1:800 in preblocking solutions) for 2 days.

The primary antibodies were: rabbit anti-FE (catalog #A889, Invitrogen; RRID:AB_221561); rabbit anti-CBL (catalog #5760, Invitrogen; RRID:AB_ 2536192); and rabbit anti-Alexa Fluor 488 (catalog #11094, Molecular Probes; RRID:AB_ 221544). After primary antibody incubation, we thoroughly rinsed the sections with PBS and then incubated them overnight in secondary antibody solution (biotinylated goat anti-rabbit IgG; catalog #BA-1000, Vector Laboratories; RRID:AB_2313606) at 1:200 in preblocking solution at 4 °C, followed by avidin–biotin horseradish peroxidase (AB-HRP; catalog #PK-6100, Vector Laboratories; RRID:AB_2336827) at a 1:100 dilution in PBS for 1 h, and then processed with DAB for 2–3 min (catalog #SK-4100, Vector Laboratories; RRID:AB_2336382). During antibody incubation, we microwaved (BioWave, Ted Pella) the tissue sections twice a day (3 min on, 2 min off, 3 min on, at 150 W) to enhance antibody penetration. After DAB, we mounted the tissue on gelatin-coated glass slides and left to dry for more than 10 days. We stained every other section with Nissl and coverslipped mounted sections with Entellan Mounting Medium, as described previously (Wang and Barbas 2018).

Tissue Processing To Study Appositions With Inhibitory Neurons: Immunofluorescence (Goals 2 and 3)

For goal 2, we double-labeled tissue sections at the level of A25 with tracers and one of the calcium-binding proteins to visualize two antigens simultaneously. Free-floating sections went through antigen retrieval, glycine incubation, and preblocking, as described above. We then incubated tissue sections with antibodies for tracers (rabbit anti-FE, or rabbit anti-CBL or rabbit anti-Alexa Flour 488) at 1:800 and calcium-binding proteins (mouse anti-CR [catalog #6B3, Swant; RRID:AB_10000320] or mouse-anti-PV [catalog #235, Swant; RRID:AB_10000343]; or mouse-anti-CB [catalog #300, Swant; RRID:AB_ 10000347]) at 1:2000 in preblock solution for 2 days. Then, the tissue sections were rinsed with 0.01 M PBS and incubated overnight with secondary antibodies conjugated with fluorescent label. The tracers were visualized with either green or blue fluorescence (Alexa Fluor 488 goat anti-rabbit IgG [catalog #A11008, Invitrogen; RRID:AB_143165] or Alexa Fluor 405 goat anti-rabbit IgG [catalog #A31556, Invitrogen; RRID:AB_ 221605]). Calcium-binding proteins were visualized with far red fluorescence to avoid photo bleaching (Alexa Fluor 647 goat anti-mouse IgG [catalog #A21235, Invitrogen; RRID:AB_2535804]) at 1:100 in preblocking solutions. We then rinsed tissue sections with 0.1 M PB, mounted them on gelatin-coated glass slides, dried them overnight, and coverslipped them with Prolong Gold Antifade Mounting Medium (catalog #36930, Invitrogen). Tissue sections were microwaved twice a day for primary and secondary antibody incubation steps. We omitted either the primary or the secondary antibody for control experiments and found no evidence of immunolabeling.

For goal 3, we labeled tissue sections at the level of A25 with tracer and D1 receptors in one case (BT) and D1 receptors alone in two cases (BH and BI). The procedure was similar as above. For double-labeling, we used primary antibodies against the D1 receptor (1:800, rat anti-D1 receptor, catalog #D2944, Sigma; RRID:AB_ 1840787) and against the tracer (1:800, rabbit anti-FE), and secondary antibodies (1:100, Alexa Fluor 568 goat anti-rat IgG, catalog #A11077, Invitrogen; RRID:AB_ 2534121, and Alexa Fluor 488 goat anti-rabbit IgG). To view the distribution of D1 receptors only ($n = 2$ cases), we used an antibody for the D1 receptor (primary antibody: 1:800, rat anti-D1 receptor; and secondary antibody:1:100, Alexa Fluor 568 goat anti-rat IgG).

Tissue Processing For Electron Microscopy (Detailed Methods: Goals 2 and 3)

We first mounted sections on glass slides and photographed them with a CCD camera mounted on a microscope (model BX51, Olympus) to obtain a fresh tissue map and fiduciary marks for subsequent processing for EM. We chose tissue sections with dense hippocampal terminations in A25, based on the pathway distribution (studied above) to yield enough signal in small sections (maximum: $1000 \times 1000 \times 50$ µm) for EM analyses at high resolution. Double or triple immunohistochemistry staining for tracer- and calcium-binding proteins or D1 receptors was performed first to label the antigens with distinct elements for identification (tracers with DAB [dark uniform precipitate], calcium-binding proteins with gold [black dots] or tetramethylbenzidine [TMB, black crystal rods], and D1 with TMB), and then followed by processing to infiltrate heavy metals into the tissue to visualize with EM. Each tissue section was labeled with two antigens for double-labeling or three antigens for triple-labeling in order to simultaneously visualize the tracer and one or two calcium-binding proteins or the D1 receptor in the same tissue.

For double-labeling, free-floating sections went through glycine incubation, hydrogen peroxide incubation, AB blocking, and primary antibody incubation, as described above. The only difference was in the preblock solution for the primary antibody incubation, which contained reduced Triton X-100 (0.025%, Roche Applied Science) to help preserve the fine structure. Then, we incubated the tissue sections with secondary antibodies (1:50; UltraSmall ImmunoGold F(ab) fragment of goat anti-mouse IgG; catalog #800.266, Aurion; [RRID:AB_2315632]) in a buffer solution (10% normal goat serum, 10% BSA, 0.2% BSA-c, 0.025% Triton X-100 [Roche Applied Science], and 0.1% cold water fish gelatin [Aurion] in 0.1 M PB) and biotinylated goat anti-rabbit overnight. After incubation with secondary antibodies we fixed tissue sections with low-glutaraldehyde (3% glutaraldehyde and 1% paraformaldehyde in 0.1 M PB with a microwave session [2 min at 150 W, 4 °C]), washed them with glycine (0.05 M in 0.1 M PB, 5 min), rinsed them with PB (0.1 M), and incubated them in enhancement conditioning solution (1:10, 10 min, Aurion). We then applied silver enhancement kit for 90 min (R-Gent SE-EM, Aurion) to enhance the appearance of gold particles, and stopped the reaction with 0.1 M PB rinses followed by AB-HRP incubation and DAB, as described above. After DAB, we quickly checked DAB labeled hippocampal axons in A25 and marked the areas with dense terminations from the fresh tissue map acquired before processing.

The procedure of triple-labeling is similar to the double-labeling described above, with changes in primary and secondary antibodies and addition of TMB staining. Briefly, free-floating sections were incubated with primary antibodies for tracers, and for two of the calcium-binding proteins (mouse anti-PV, mouse anti-CB, goat anti-CR [catalog #CG1, Swant; RRID:AB_10000342]) or incubated with primary antibodies for tracers, calretinin (goat anti-CR), and D1 receptors. After 2 days in primary antibody incubation, we incubated tissue sections overnight with secondary antibodies (biotin-SP donkey anti-rabbit [1:200, catalog # 711-065-152, Jackson; RRID:AB_2340593], ultra-small gold conjugated donkey anti-mouse [1:50; catalog #800.322, Aurion], and gold conjugated donkey anti-goat antibody [1:50; catalog #800.333, Aurion]). The primary and secondary antibodies were diluted in buffer solution with normal donkey serum. Then tissue sections went through low-glutaraldehyde fixation, glycine wash, PB rinse, enhancement conditioning solution, silver enhancement kit incubation,

followed by AB-HRP incubation and DAB, as described above. After DAB staining, we thoroughly rinsed the tissue sections with 0.1 M PB, incubated them with hydrogen peroxide (5 min) and AB blocking solutions to block remaining HRP-binding sites. We then incubated the tissue sections with the third secondary antibody (Peroxidase-AffiniPure donkey anti-rat [1;200; catalog #712-035-150, Jackson, RRID:AB_ 2340638] or Peroxidase-AffiniPure donkey anti-goat [1;200; catalog #705-035-003, Jackson, RRID:AB_ 2340390]) overnight. Then tissue sections went through TMB staining and then stabilized with DAB-cobalt chloride solution, as described previously (Medalla et al. 2007). In control experiments, we omitted primary or secondary antibodies and found no immunohistochemical labeling.

We then used block-face imaging EM processing to introduce heavy metals into the tissue. We first postfixed tissue sections with 6% glutaraldehyde and 2% paraformaldehyde in 0.1 M PB in a microwave oven (150 W at 15 °C) until the sample temperature reached 30–35 °C, and then rinsed sections with PB thoroughly. Tissue sections then went through reduced osmium staining (1% osmium tetroxide [Electron Microscopy Sciences] with 1.5% potassium ferrocyanide [Electron Microscopy Sciences] in dH_2O with a microwave session [100 W at 4 °C; 6 min under vacuum]), post staining for an additional 5 min, and dH_2O rinses (3× 5 min). We then incubated the tissue sections in 1% thiocarbohydrazide in dH_2O (Sigma-Aldrich) for 30 min, rinsed them with dH_2O (3× 5 min), and stained them with a second osmium solution (1% osmium tetroxide in water) under vacuum for 6 min and postfixed for an additional 5 min. After three water rinses, tissue sections were incubated in 1% uranyl acetate in dH_2O (Electron Microscopy Sciences) overnight at 4 °C. On the second day, tissue sections first went through dH_2O rinses (3× 5 min), lead aspartate incubation for 30 min at 60 °C (0.066 g lead nitrate [Electron Microscopy Sciences] dissolved in 10 mL of 0.4% L-aspartic acid in dH_2O, pH 5.5), and dehydration steps in ascending graded ethanols (50%, 75%, 85%, 95%, 100%; 3× 5 min each). We then infiltrated the tissue sections with propylene oxide (2× 10 min; Electron Microscopy Sciences), and ascending graded LX112 resin-propylene oxide mix (1:1 for 1 h and 2:1 overnight, LX112 Embedding Kits, Ladd Research Industries). The following day we infiltrated the tissue sections with pure LX112 resin for 4 h under vacuum, flat embedded them in LX112 resin in Aclar (Ted Pella), and cured for ≥48 h at 60 °C.

Hippocampal Bouton Analysis Used With 2D and 3D Electron Microscopy (Goals 2 and 3)

To select tissue for EM with hippocampal terminations in the upper and deep layers of A25, we used fiduciary landmarks (e.g., blood vessels) from maps acquired after DAB staining (described above). We cut small cubes (maximum: 1000 × 1000 × 50 µm) of Alcar-embedded tissue with the aid of a stereomicroscope. For tissue sections to view in a transmission EM (100CX, JEOL) with a digital camera (DigitalMicrograph, GATAN), we placed the small cubes of tissue on top of premade LX112 resin blocks with fresh LX112 resin and cured them for ≥48 h at 60 °C. These tissue sections were then cut in 50 nm thickness with an ultramicrotome (Ultracut UCT, Leica Microsystems). The series of ultrathin sections were collected in order on pioloform-coated copper slot grids. We searched for hippocampal boutons in these ultrathin section EM series, and captured them at ×33 000 magnification across at least 5 sections.

For block-face imaging, we used 3View 2XP System (GATAN) coupled to a 1.5 KV scanning electron microscope (GeminiSEM 300, Zeiss). The small cubes of tissues were glued onto aluminum pins with conductive epoxy glue (catalog #CW2400, Chemtronics). We then cut the extra resin to expose the tissue surface using an ultramicrotome, and coated the edge of the specimen with silver paint (catalog #16035, Ted Pella) to reduce charging. We then mounted the aluminum pins in the 3view 2XP system, which has a built-in ultramicrotome to cut the surface of the sections in 50 nm thickness. A back-scattered detector captured series of images (20 × 20 to 25 × 25 µm fields at 6.5 nm for 50–200 section series). We used all hippocampal boutons in the images for analysis. Using these two methods, we used the hippocampal boutons that had complete profiles for 3D EM analyses and the ones with incomplete profiles for 2D EM analyses.

Data Analysis

Brightfield Microscopy: Axon Tracing, Unbiased Stereology and Bouton Size (Goals 1 and 2)

We first outlined areas and layers in ACC in series of sections with hippocampal terminations labeled with DAB (1 in 40 sections) for each of two cases (cases BQ and BT). We then exhaustively traced labeled hippocampal axons with boutons (at ×400 magnification) within the outlined areas of interest in ACC using a semiautomated work-station (StereoInvestigator, version 10 and a model BX60 camera, Olympus America). The maps of hippocampal axons in ACC helped to show their distribution qualitatively.

We then used unbiased stereologic methods to study the distribution of hippocampal axon boutons quantitatively (West 2012). We used a semiautomated system (StereoInvestigator) to sample hippocampal axon boutons in the upper and deep layers of A25, A32, and A24a in one series of sections (1 in 20 sections) for each case. To randomly sample hippocampal terminations and reach sufficient sampling (Gundersen error $[m = 1] \leq 10\%$), we used a counting frame of 50 × 50 µm, a disector height of 2–5 µm, and a varied grid spacing (50 × 50 µm, 100 × 100 µm, 500 × 500 µm) depending on the density of the hippocampal terminations. We used high magnification (×1000) to ensure that only labeled hippocampal axon boutons were sampled. We calculated the number of hippocampal boutons and volume of each region and layer using stereologic analyses.

To measure bouton size using brightfield microscopy, we acquired stacks of images from the upper and deep layers of A25, A32, and A24a and imported the stack of images into the software system Reconstruct (SynapseWeb; RRID:SCR_002716; Fiala 2005). We circled all hippocampal boutons in the stack of images using the program Reconstruct and measured the major diameter for each circled hippocampal bouton. We measured >1000 boutons for each case in the upper and deep layers of A25, A32, and A24a.

EM and Confocal Analysis of Postsynaptic Sites (Goal 2)

We also calculated the major diameter of hippocampal boutons in the upper and deep layers of A25 using 2D and 3D EM images (described above). The image stacks were imported into Reconstruct and each bouton was circled at maximum size with appearance of the synapse.

We recorded the presence of mitochondria and types of PSD (round or perforated) using all hippocampal boutons found in the upper and deep layers of A25 in EM. Only hippocampal boutons with complete profiles were used to calculate bouton volume and PSD surface area.

We calculated the proportion of hippocampal boutons that apposed calcium-binding protein positive elements versus those that did not, using stacks of images acquired in a confocal microscope (model LSM 880 microscope, Zeiss). The apposition site was the area of colocalization at the point of contact, viewed consistently at varied angles of rotation. To reduce blurring, we used deconvolution for each stack (AutoDeblur X software, Media Cybernetics; RRID:SCR_002465). We also examined all hippocampal boutons acquired with EM for features of their postsynaptic targets, including dendritic shafts, spines, synapses at more than one site, and synapses on calcium-binding protein positive postsynaptic elements. To determine the nature of the postsynaptic targets, we calculated spine density and synapse density on dendritic shafts using 3D EM.

Analyses of the Relationship Between Hippocampal Terminations and D1 Receptors (Goal 3)

We acquired image stacks with the same thickness from three cases using confocal microscopy (cases BT, BI, and BH). For each case, we used the same parameters for confocal microscopy and randomly acquired six image stacks from the upper and deep layers of A25. To estimate D1 receptor expression levels in the confocal image stacks, we first removed background noise using a pixel brightness threshold. We also removed labeled pixel clusters that were above threshold but smaller than a criterion size. The threshold for acceptance of pixel clusters as D1 receptor label varied by case due to experimental variability, but was consistent for the upper and deep layer image stacks from a given case. For the three cases used, the thresholds used were 30, 20, and 60 (out of a maximum channel brightness of 255). In all cases, contiguous pixel clusters smaller than 25 pixels in size were removed. We calculated the ratio of D1 expression in deep versus the upper layers from the denoised image stacks in 2 ways: the total number of above-threshold pixel clusters in each image stack, and the average density of labeled pixels per image stack. Analysis was performed using custom code written in MATLAB (R2018b, Mathworks, Inc.).

We used the EM sections to calculate the proportion of spines with D1 receptors that received hippocampal terminations in the upper and deep layers of A25 in 2 cases (cases BQ and BT). For control experiments, we omitted primary and secondary antibodies and found no D1 positive labeling. Even though we saturated the remaining binding sites before applying secondary antibodies for TMB (D1 receptor), we cannot rule out the possibility of nonspecific labeling of D1 receptors. Therefore, we focused on postsynaptic D1 receptors, which were present around dendritic spines innervated by hippocampal labeled boutons. The relationship between hippocampal terminations and D1 receptors was similar between the 2 cases, even though one case yielded a smaller sample for analysis based on the comparatively low density of hippocampal terminations in the available tissue ($n = 11$ boutons in case BQ).

Statistics

We compared the proportion of hippocampal boutons in each area across cases (cases BQ, BS, BT, and BU) using ANOVA with Bonferroni's post hoc test. We used two-tailed *t* tests for paired comparison, including bouton diameters, volumes, PSD areas, morphologic features, and types of postsynaptic targets of hippocampal boutons between upper and deep layers of A25. We used linear regression for PSD surface area and bouton volume or diameter. We used SPSS software (IBM; RRID:SCR_002865) for all statistical analyses.

Results

Injection Sites

The hippocampus is a complex structure that can be subdivided into anterior and posterior sectors, subregions, and layers (reviewed in Amaral and Lavenex 2006). Details of the architecture of the rhesus monkey hippocampus can be found in previous studies (Bakst and Amaral 1984; Rosene and Van Hoesen 1987; Wang and Barbas 2018). To provide context for our findings, we include a summary map (Fig. 1*B*), which depicts the regions and layers of the hippocampus that we had recently analyzed in detail (Wang and Barbas 2018).

We focused on the projections from CA subregions and the prosubiculum of the anterior sector of the hippocampus, because projection neurons to ACC in rhesus monkeys originate mostly from these sites (Barbas and Blatt 1995; Munoz and Insausti 2005). A summary of our experimental approach is shown in Figure 1*A*.

To study the pathways from hippocampus to ACC, we injected neural tracers in four rhesus monkeys (Fig. 1). The details of the extent of the injection sites are listed in Table 1. Briefly, the neural tracer in case BQ (Alexa488) was concentrated in all layers of part of ventral CA1 and the nearby prosubiculum and impinged on the dentate gyrus. The tracer in case BT (FE) included all layers of the ventral part of CA1 and impinged on the dentate gyrus and CA3. In two other cases, the tracer injected in the hippocampus was CBL. In one of these (case BS), the injection site included the layers RAD and PCL of the ventral part of CA1. In another case (BU), the injection included all layers of the dentate gyrus and SLM and RAD layers of all CA fields.

Distribution of Hippocampal Terminations in ACC

We conducted a detailed analysis of hippocampal terminations in ACC areas (A25, A32, and A24a), which receive the most robust unidirectional pathways from the hippocampus among prefrontal areas (Aggleton et al. 2015). These three cortical areas are situated on the medial wall of the prefrontal cortex (Fig. 1*A*), with A25 extending to the medial orbital surface. The architecture of these ACC areas is dysgranular (Fig. 2*A*), characterized by an incipient layer IV (Barbas and Pandya 1989; Joyce and Barbas 2018).

We first mapped hippocampal axon terminals exhaustively through short intervals from anterior to posterior levels in A25, A32, and A24a in two cases (BQ, Fig. 2*B* top panels; BT, Fig. 2*B* bottom panels). The pattern of hippocampal terminations was similar in the two cases, with the densest axon terminals found in mid-to-posterior A25, especially in its orbital part. Additionally, we saw a slight trend with a preference of hippocampal axons innervating the upper layers (layers I, II, III) within the comparatively sparse terminations in the anterior to mid-level of A25. By contrast, the most robust terminations in posterior levels of A25 preferentially innervated the deep layers (layers V and VI; Fig. 2*B*). This trend seems to parallel the cytoarchitectonic gradient in A25, where layer IV is slightly denser in its anterior than its posterior sector (Mackey and Petrides 2014; Garcia-Cabezas et al. 2017).

We then investigated quantitatively hippocampal terminations (boutons, example in Fig. 2*C*) using unbiased stereologic

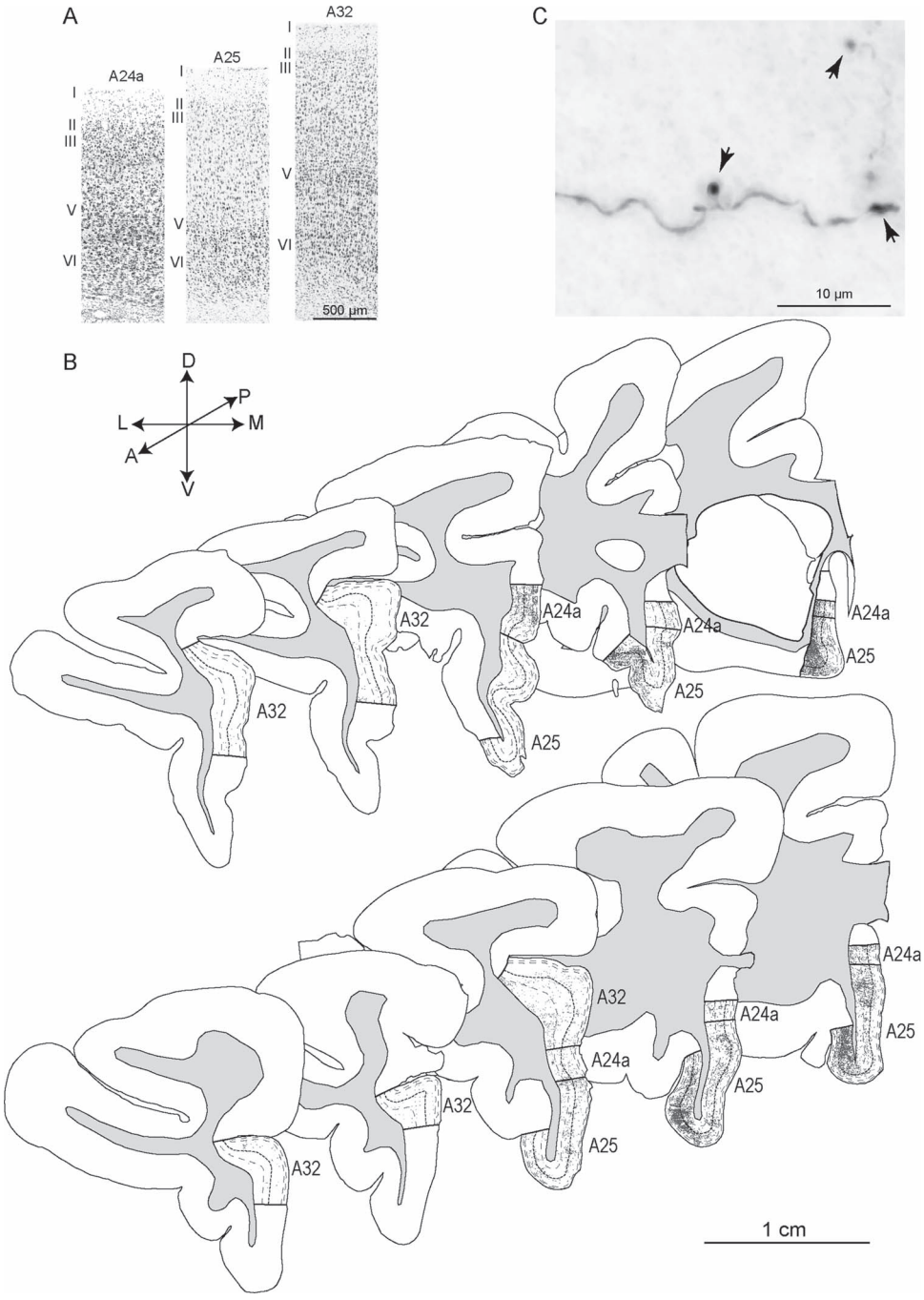

Figure 2. Architecture of ACC areas and hippocampal axon terminals. (*A*) Photomicrographs of cortical columns from A24a, A25, and A32 stained with Nissl show the cytoarchitecture. (*B*) Diagrams of coronal sections show the distribution of labeled hippocampal axon terminals (dark gray) in A24a, A25, and A32 (case BQ, top panel; case BT, bottom panel) from anterior to posterior levels (left to right). The thick dotted lines indicate borders between upper (I–III) and deep (IV–VI) layers; thin dotted lines show border between layers I, II and III (upper) and V and VI (deep). Gray shade depicts the white matter. (*C*) Grayscale photomicrograph through A25 shows labeled hippocampal axon terminals (boutons, arrows). Scale bars: A, 500 µm; B: 1 cm; C: 10 µm.

methods in four cases and the results are shown in Figure 3. About 60% of hippocampal axon boutons were found in A25 (Fig. 3A), followed by A32 ($26.5 \pm 10.9\%$, mean $\pm$ SE) and then A24a ($14.8 \pm 4.1\%$). The proportion of hippocampal axon boutons in A25 was significantly higher than in A24a (one-way ANOVA $F_{(2,9)} = 5.069$, $P = 0.034$, with Bonferroni's post hoc test, A25 vs. A24a: $P = 0.04$), and showed only a higher trend that was not statistically significant when compared with A32 (Bonferroni's post hoc test, A25 vs. A32: $P = 0.151$). Since these areas differ in volume, we also calculated the density of hippocampal axon boutons. A25 had the highest bouton density compared with A32 and A24a in three cases (Fig. 3B). In one case (BU), the hippocampal bouton density was similar in A24a and A25, and higher than in A32, a pattern that may reflect the placement of the injection

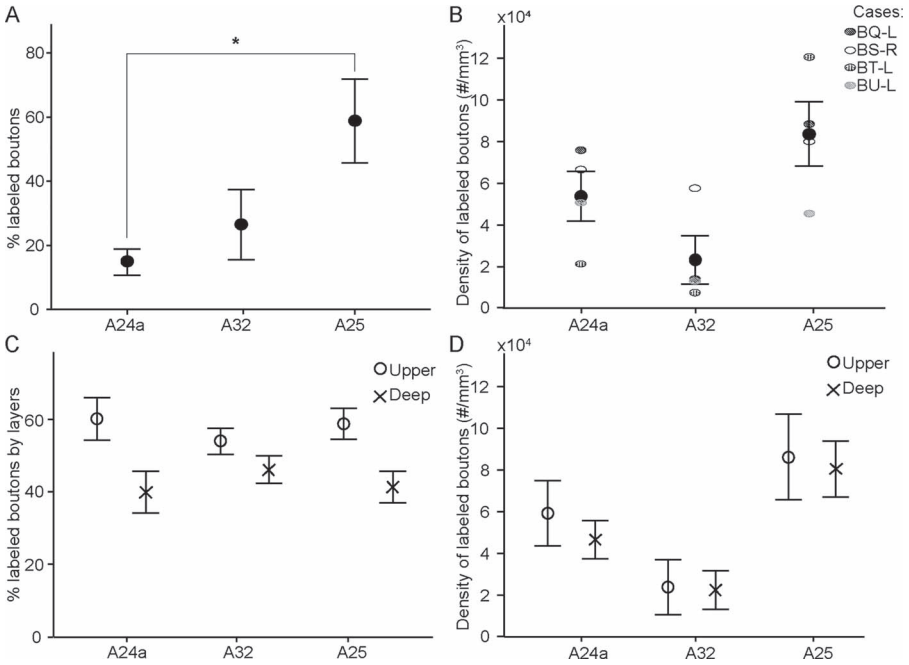

Figure 3. Stereologic analysis of hippocampal boutons in ACC. (*A*) Proportion of hippocampal boutons in A24a, A32, and A25; ∗ statistically significant comparisons. (*B*) Density of hippocampal boutons in A24a, A32, and A25. (*C*) Proportion of hippocampal boutons in the upper (circles) and deep (crosses) layers in each area. (*D*) Density of hippocampal boutons in upper (circles) and deep (crosses) layers in each area. Error bars: ±SE.

in proximal CA1 (Fig. 1, case BU). Stereologic analysis confirmed that the proportion and density of hippocampal axon boutons was similar in the upper and deep layers for all three ACC areas, consistent with the pattern shown with the axon tracing method (above). These findings thus showed that A25 is the preferred target of hippocampus among the ACC areas, and both upper and deep layers of ACC receive hippocampal terminations.

The Size of Hippocampal Boutons was Similar Across ACC Areas and Layers

Several presynaptic and postsynaptic features correlate with synaptic efficacy. At the presynaptic level, large boutons contain more synaptic vesicles and have higher probability of multivesicular release upon stimulation (Stevens 2004; Germuska et al. 2006). We thus measured the diameter of hippocampal boutons in A25, A32, and A24a under brightfield illumination. The results showed that the size of hippocampal boutons in these three regions was similar (one-way ANOVA, $F_{(2,9)} = 1.133$, $P = 0.364$, $n = 35\,805$, from four cases; Fig. 4A,B), as well as for the upper and deep layers ($P > 0.05$).

We then studied the hippocampal pathway at the synaptic level in A25, which was the major target of the hippocampus in ACC. Analyses in 2D and 3D of EM images showed similarity in the major diameter and bouton volume of hippocampal boutons in the upper and deep layers (for diameter: 2D EM: $t_{(4)} = 1.207$, $P = 0.113$, $n = 509$, from three cases; 3D EM: $t_{(2)} = -0.076$, $P = 0.947$, $n = 387$, from two cases; Fig. 4C,D; for volume: $t_{(2)} = -0.076$, $P = 0.947$, $n = 387$, from two cases, Fig. 5A), confirming and extending our findings at the level of the system. We found that about 65% of hippocampal boutons in both the upper and deep layers of A25 have mitochondria (Fig. 5B), suggesting that this is a highly active pathway (Thomson 2000).

Synaptic efficacy is also correlated with the features of the postsynaptic elements (Peters et al. 1991; Germuska et al. 2006), such as PSD surface area, which is correlated with the density of AMPA receptors (Bourne and Harris 2008; Nava et al. 2014). Another postsynaptic feature is the shape of the synapse: perforated synapses increase the PSD surface area (Geinisman 1993; Desmond and Weinberg 1998; Medalla and Luebke 2015). Comparison of the surface area of PSD and perforated synapses (Fig. 6B) in the upper and deep layers of A25 using EM showed similar findings for hippocampal boutons in the upper and deep layers (surface area: $t_{(2)} = -0.013$, $P = 0.991$, $n = 384$, from two cases; perforated: $t_{(4)} = -0.200$, $P = 0.852$, $n = 886$, from three cases; Fig. 5C,D).

In addition, we found that about 40% of hippocampal boutons in both upper and deep layers of A25 had spine apparatus (Fig. 6B, star), a feature associated with the capacity to regulate spine calcium level (Peters et al. 1991). In summary, the size and morphological features of the hippocampal boutons in the upper and deep layers of A25 were similar.

We also found that the PSD surface area for hippocampal terminations in the upper or deep layers of A25 was significantly correlated with bouton volume (linear regression: $n = 345$ boutons, $R^2 = 0.471$, $F_{(1,1.466)} = 305.712$, $P = 0.000$), and with bouton diameter (linear regression: $n = 345$ boutons, $R^2 = 0.491$, $F_{(1,1.536)} = 334.425$, $P = 0.000$; Fig. 5E,F). These findings are consistent with patterns seen in other cortical and subcortical pathways (Germuska et al. 2006; Medalla and Barbas 2009; Wang and Barbas 2018).

Hippocampal Pathways in A25 Target Mostly Excitatory Neurons and Some CR Inhibitory Neurons

Morphological features can be used reliably to identify excitatory and inhibitory neurons at the EM level. High spine density

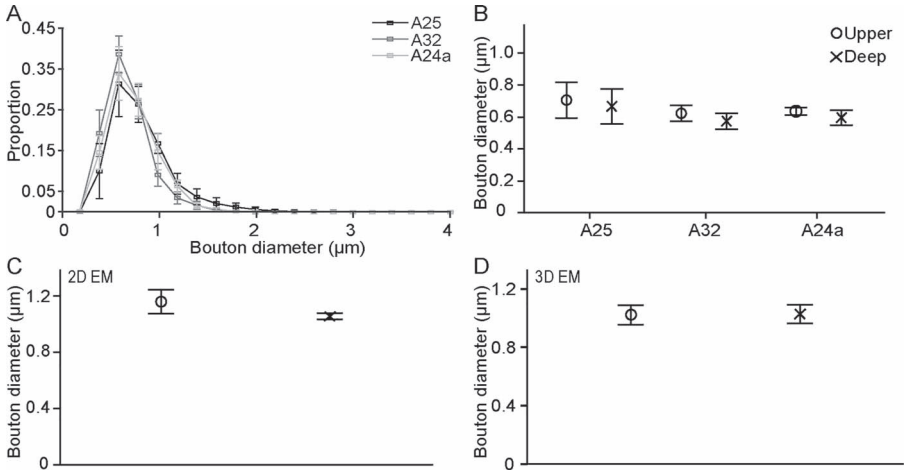

Figure 4. The size of hippocampal boutons was similar across ACC areas and between the upper and deep layers. (*A*) Bouton major diameter frequency distributions in A25, A32, and A24a. (*B*) Hippocampal boutons are similar in size across ACC and between the upper and deep layers. (*C*, *D*) Similarity in bouton major diameter in the upper and deep layers of A25 using 2D and 3D EM. Error bars: ±SE.

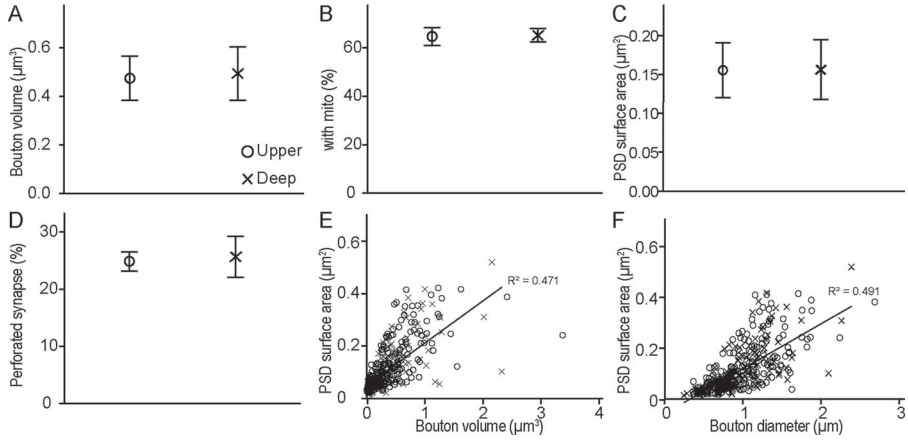

Figure 5. Presynaptic and postsynaptic features of hippocampal boutons in A25. (*A*) Hippocampal bouton volume was similar in the upper and deep layers of A25. (*B*) Proportion of hippocampal boutons that contained mitochondria (mito) and formed synapses in the upper and deep layers of A25. (*C*) PSD surface area of postsynaptic sites that receive hippocampal projections in the upper and deep layers of A25. (*D*) Proportion of hippocampal boutons that formed perforated synapses in the upper and deep layers of A25. (*E*, *F*) Relationship of PSD surface area and bouton volume (*E*) or diameter (*F*) for all cases. Upper layers, circles; deep layers, crosses. Error bars: ±SE.

at the postsynaptic site and low synapse density on dendritic shafts indicate a synapse on excitatory neurons (Peters et al. 1991). We used serial EM to investigate the type of neurons that the hippocampal pathway targets in A25. Nearly 90% of hippocampal terminations in both the upper and deep layers of A25 innervated spines found on putative excitatory neurons (Figs 7*A* and 8*G* from three cases). A small proportion of hippocampal terminations in the upper layers (2.9%, $n = 560$ boutons, 3 cases) and in the deep layers (3.6%, $n = 363$ boutons, 3 cases) formed synapses on dendritic shafts, suggesting interaction with inhibitory postsynaptic sites (Fig. 8*H*). The rest of the hippocampal boutons formed synapses on more than one spine that emerged from presumed excitatory neurons in A25 (upper layers: 5.2%; deep layers: 3.1%; Fig. 8*I*). Hippocampal terminations thus overwhelmingly innervated excitatory neurons in A25. The only two other pathways we have seen that had a similarly strong bias for innervation of excitatory targets were the ACC pathways to the olfactory cortices and to posterior orbitofrontal cortex in rhesus monkeys (García-Cabezas and Barbas 2014, 2017).

Among the small class of targeted inhibitory neurons in A25, we next investigated their type by simultaneously labeling the pathway and CB, CR, or PV, to identify which are targeted by the hippocampal pathway (Fig. 8*A*–*D*). We first double-labeled A25 sections with tracer and one of the calcium-binding proteins with different fluorescent markers to calculate the proportion of hippocampal terminations apposed with inhibitory neurons. Overall, there was a higher proportion of hippocampal terminations on CR neurons in A25. The proportion of hippocampal terminations apposed on CR, CB, and PV neurons was comparable between upper and deep layers of A25 (upper layers: CR, 3.6%, CB, 1.2%, PV, 0.1%; deep layers: CR, 3.9%, CB, 1.8%, PV, 0.4%; $n = 14\,119$, from two cases). We thus collapsed the data across layers in A25 and found an overall significant difference in hippocampal targets on elements of each of the distinct neurochemical classes of inhibitory neurons in A25 (CR, 3.81%, CB, 1.54%, PV, 0.25%, one-way ANOVA, $F_{(2,3)} = 13.526$, $P = 0.032$). Bonferroni's post hoc test revealed a statistically significant difference in the comparison of CR versus PV ($P = 0.04$), but not in the other pair comparisons ($P > 0.05$; $n = 14\,119$, from

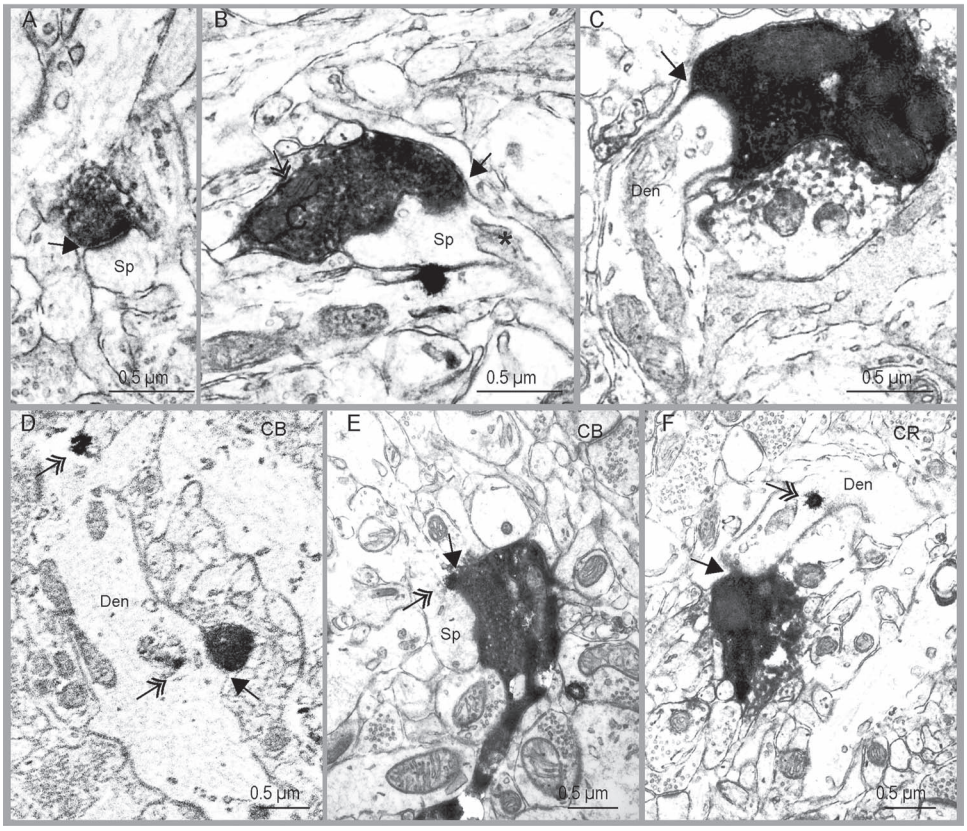

Figure 6. Varied types of hippocampal boutons and their postsynaptic targets in A25. (*A*) Example of hippocampal bouton making a round synapse (arrow) on a spine (Sp). (*B*) Example of hippocampal bouton with mitochondria (double headed arrow) making a perforated synapse (arrow) on a spine (Sp); ∗: spine apparatus. (*C*) Example of hippocampal bouton that formed a synapse on a dendritic shaft. (*D–F*) Examples of hippocampal axon boutons that formed synapses on CB or CR positive elements. *D*, hippocampal bouton forming a synapse on CB positive dendritic shaft (double-headed arrow shows CB label in dendrite, Den); *E*, hippocampal bouton forming a synapse on a CB positive spine; *F*, hippocampal bouton forming a synapse on CR positive dendritic shaft. Black arrows show the synaptic sites. Double-headed arrows indicate the gold labeling for CB or CR. Abbreviations: Sp, spine; Den, dendritic shaft. Scale bar, 0.5 µm.

two cases, Fig. 7*B*; asterisk shows statistically significant difference).

We then investigated the hippocampal pathway interaction with inhibitory neurons at the synaptic level. We used double or triple immunohistochemistry followed by EM processing to label the tracer- and calcium-binding proteins (Fig. 6*D–F*). We found a similar trend in the EM analyses (upper: CR, 2.4%, CB, 1.2%, PV, 0%; deep: CR, 2.5%, CB, 1.4%, PV, 0%, $n = 1118$ synapses, from two cases; collapsed across layers in Fig. 7*C*). We did not find any hippocampal axon boutons that formed a synapse on PV labeled neurons in either the upper or deep layers of A25. This finding is consistent with the low proportion of hippocampal terminations apposed on PV neurons found at the confocal level (above). Additionally, as shown in Figure 8*A–D*, in A25 PV neurons are sparser than CB and CR neurons and their dendritic arborization is not as elaborate as CB and CR neurons, as also reported previously (Dombrowski et al. 2001; Garcia-Cabezas et al. 2017; Joyce and Barbas 2018).

We also used morphologic criteria to study hippocampal terminations on postsynaptic targets in the EM, where several morphologic features can be used to identify presumed inhibitory postsynaptic sites. One of these includes aspiny or sparsely spiny dendrites (Peters et al. 1991). Another is the presence of frequent synapses on dendritic shafts. In prefrontal cortex of the rhesus monkey, studies have shown that aspiny and sparsely spiny dendrites with spine density <0.5 spines/µm and 2–0.6 synapses on dendritic shaft/µm likely belong to inhibitory neurons (e.g., Medalla and Barbas 2009). We thus used these morphologic criteria as well as three calcium-binding proteins that label inhibitory neurons in the primate cortex (DeFelipe 1997) to categorize the postsynaptic elements. In our samples, the sparsely spiny dendritic shafts and CR labeled dendrites that received hippocampal inputs had spine density of <0.20 spines/µm and synapse density on the shaft of 0.19–2.78 synapses/µm, suggesting that these dendrites belong to inhibitory neurons. About half of the hippocampal terminations that innervated CB postsynaptic sites were found on dendritic shafts (Fig. 6*D*), and the other half innervated CB labeled spines (Fig. 6*E*, double arrow). All CB positive dendritic shafts that received hippocampal terminations were aspiny or sparsely spiny (synapse density on dendritic shaft: 0.60–0.79 synapses/µm), and were presumed to be inhibitory neurons. We then followed CB positive spines back to their dendritic shaft and calculated spine density (0.28 spines/µm) and synapse density on dendritic shafts (0.49 synapses/µm).

Studies have shown that most of the CB neurons in the monkey cortex coexpress GABA (Gabbott and Bacon 1996a, 1996b; DeFelipe 1997; Rocco et al. 2016), but a small proportion of pyramidal neurons contain light CB labeling in the monkey cortex (Gabbott and Bacon 1996a; Kondo et al. 1999), reviewed

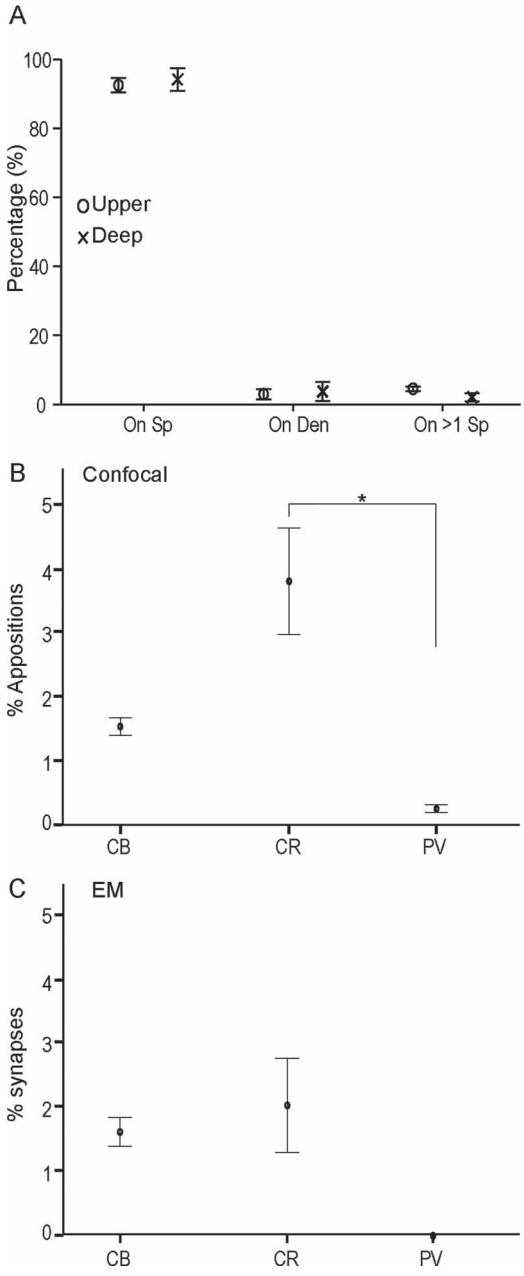

Figure 7. Postsynaptic targets of hippocampal terminations in the upper and deep layers of A25. (*A*) Proportion of hippocampal boutons that formed synapses with three categories of postsynaptic targets (on spine, Sp; on dendritic shaft, Den; or on more than one spine, on >1 Sp). Upper layers, circles; deep layers, crosses. (*B*) Plots show the proportion of hippocampal terminations apposed on one of three neurochemical classes of inhibitory neurons labeled with calcium-binding proteins in A25; ∗, statistically significant comparisons. (*C*) Plots show the proportion of hippocampal axon boutons that formed synapses on postsynaptic elements labeled with calcium-binding proteins in A25. In *B* and *C*, layers were collapsed. Error bars: ±SE.

in (Barbas et al. 2018). It is thus not possible to rule out that a small proportion of CB labeled postsynaptic sites may be on pyramidal neurons. In summary, among the small number of targeted labeled postsynaptic sites for inhibitory neurons, the hippocampal pathway preferentially targeted CR inhibitory neurons. A small number also formed synapses on CB neurons, and showed only sparse apposition with PV neurons in A25.

Hippocampal Terminations in A25 may be Modulated by Dopamine via D1 Receptors

Several studies in primates have shown that D1 receptors are abundant in the prefrontal cortex (Lidow et al. 1991; Smiley et al. 1994; Palomero-Gallagher et al. 2009). Further, studies in rats and mice have shown that hippocampal inputs to mPFC are modulated by activation of D1 receptors (Gurden et al. 1999; Seamans and Yang 2004).

We first investigated the distribution of D1 receptors in A25 using confocal microscopy. D1 receptors were found in both the upper and deep layers of A25, with a bias towards the deep layers (Fig. 9A,B). To assess the degree of bias, we analyzed confocal image stacks to compare the degree of staining by the D1 receptor label. We employed two stages of filtering to remove background noise. We then calculated the ratio of D1 expression in deep versus upper layers from the processed image stacks in two ways: using the total number of above-threshold pixel clusters in each image stack (deep: upper $= 2.7 \pm 0.7$, 3 cases, mean $\pm$ SE), and using the average density of labeled pixels per image stack (deep: upper $= 4.3 \pm 2.0$, 3 cases). This ratio was higher than the corresponding neuronal density ratio in primate A25 (deep: upper ≈ 1.3; Dombrowski et al. 2001; Mackey and Petrides 2014). This evidence suggests that the bias in D1 receptor expression for the deep layers of A25 compared with the upper layers cannot be attributed to differences in neuronal density, which is higher in the deep than in the upper layers of A25 (Dombrowski et al. 2001).

We then investigated at the synaptic level whether there are interactions between hippocampal terminations and D1 receptors in A25. We double labeled hippocampal terminations and D1 receptors in EM (Fig. 9C,D). In one case (BT), we found that 30.2% of the hippocampal terminations targeted spines that contained labeled D1 receptors in the deep layers of A25, which was higher than for the upper layers (11.6%, $n = 86$). We found a similar trend in another case (BQ), in which 4 out of 5 (80%) hippocampal boutons formed synapses on spines that contained D1 receptors in the deep layers, and 1 out of 6 (17%) did so in the upper layers.

Because the presence of mitochondria suggests active boutons (Thomson 2000), we also calculated the proportion of boutons with mitochondria in the hippocampal pathway that innervated spines with D1 receptors. We found that all of these boutons contained mitochondria in the upper layers and 84.6% in the deep layers. In summary, these results suggest that while the hippocampal terminations have a close relationship with D1 receptors in both the upper and deep layers, they may be more strongly modulated by D1 receptors in the deep layers of A25.

Discussion

We found that in rhesus monkeys the hippocampal pathways to ACC preferentially innervated A25. Within A25, the hippocampal terminations showed a preference for the upper layers in the anterior to mid-levels of A25, and for the deep layers in the more densely targeted posterior A25. Hippocampal terminations in A25 primarily innervated excitatory neurons in both the upper and deep layers. The anterior hippocampus is known to be involved in context processing (Strange et al. 2014; Eichenbaum 2017; Bachevalier 2019) and A25 is involved in emotion regulation, conflict detection, and motivation (Alexander et al. 2019a). Our findings thus suggest that the hippocampus-to-A25 pathway can mediate contextual modulation of emotion and motivation. In addition, the hippocampal terminations in

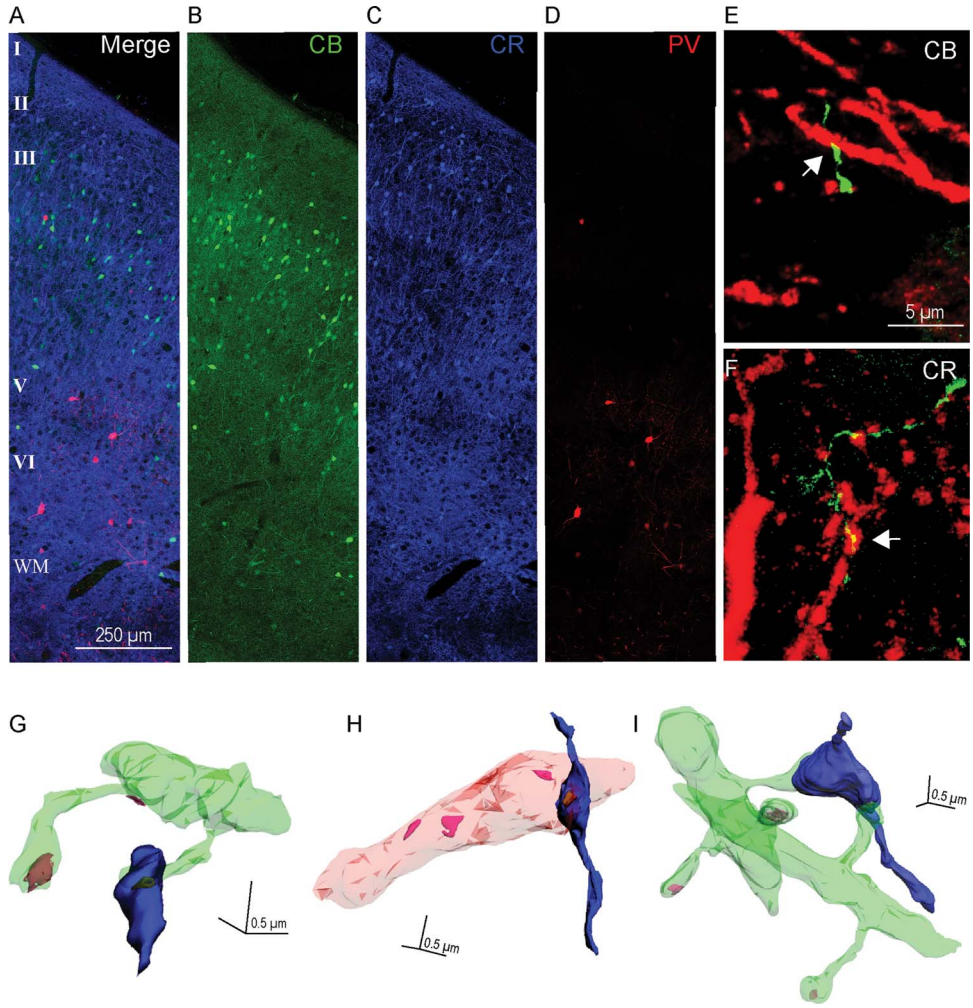

Figure 8. Relationship of hippocampal terminations to inhibitory neurons in the upper and deep layers of A25. (*A–D*) Immunofluorescence photomicrographs of three adjacent sections of A25 labeled with CB (green), CR (blue), and PV (red). (*A*) Superimposed sections (*B–D*) show all three neurochemical classes of inhibitory neurons. Scale bar, 250 µm. (*E–F*) Immunofluorescence photomicrographs show apposition sites between hippocampal terminations (green) and CB (*E*) or CR (*F*) positive elements (red); white arrows indicate apposition sites. Scale bar, 5 µm. Error bars: ±SE. (*G–I*) 3D reconstruction of labeled hippocampal boutons (blue) and their postsynaptic targets. (*G*) A hippocampal bouton forming a synapse on a spine (green). (*H*) A hippocampal bouton forming a synapse on an aspiny dendritic shaft (pink) of a presumed inhibitory neuron. (*I*) A hippocampal bouton forming a synapse on two spines that come from two distinct dendritic shafts. Color codes: green, spiny dendrites; pink, aspiny dendrite of a presumed inhibitory neuron; yellow–brown, PSD; magenta, PSD by unlabeled postsynaptic sites on dendrite; scale bar: 0.5 × 0.5 × 0.5 µm.

the deep layers of A25 may be more strongly modulated by dopamine via D1 receptors than in the upper layers. The deep layers of A25 send broadly distributed projections to many cortical areas (Joyce and Barbas 2018) and subcortical structures, including those involved in goal-directed actions and emotional expression (Haber et al. 1995; Phillips et al. 2003; Gabbott et al. 2005; Ghashghaei et al. 2007), reviewed in (Berke 2018; Van der Weele et al. 2019). The stronger dopaminergic modulation of hippocampal terminations in the deep, compared with the upper, layers has important implications for the role of the hippocampal pathway to regulate motivational processes and emotional expression.

The Hippocampal Pathway Most Robustly Targets A25 of the ACC

We found that A25 receives more and denser hippocampal terminations than A32 or A24a, especially in the mid-to-posterior levels of A25, consistent with previous findings in monkeys (Barbas and Blatt 1995; Aggleton et al. 2015). As suggested in several studies, the rodent mPFC may correspond with primate ACC (Vogt et al. 2013; Heilbronner et al. 2016), though homologies between these species are difficult to make. Nevertheless, the overall hippocampal innervation of mPFC in primates and rodents is similar. In rodents, projection neurons originate in the temporal two thirds of the hippocampus, which preferentially target the PL and IL regions of the mPFC, with a slight bias towards IL (Jay and Witter 1991; Jay et al. 1992; Verwer et al. 1997; Liu and Carter 2018).

Studies in rodents and primates have shown that the anterior hippocampus (ventral in rodents) has a close relationship with the amygdala and the hypothalamic–pituitary–adrenal axis, and contains a high concentration of hormones and neurotransmitters that modulate responses in contextual fear conditioning (Siegel and Tassoni 1971; Gage and Thompson 1980; Amaral 1985; Saunders et al. 1988; Jacobson and Sapolsky 1991; Pitkanen

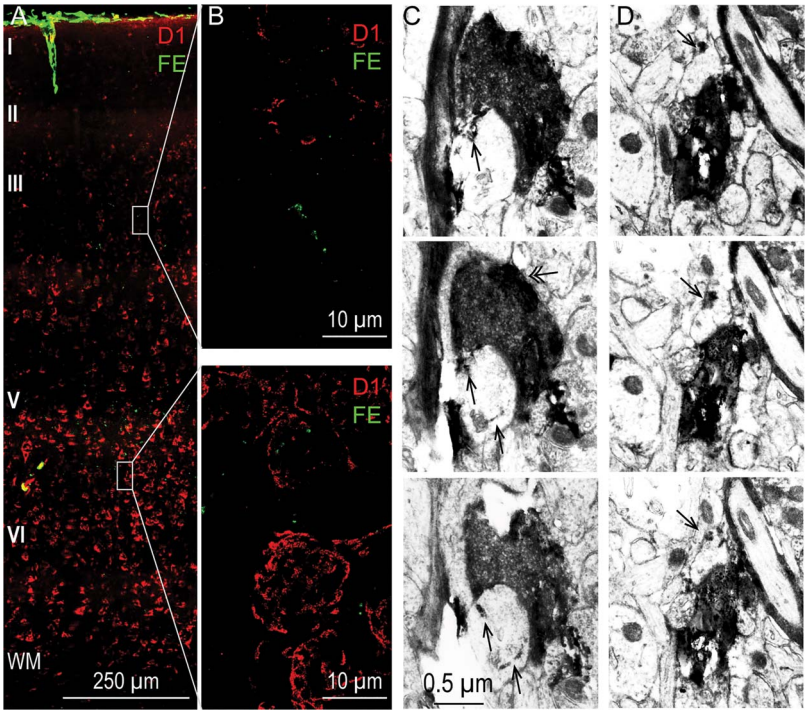

Figure 9. Relationship of hippocampal terminations to D1 receptors in the upper and deep layers of A25. (*A*) Photomicrograph of cortical column through A25 processed for D1 receptors using immunofluorescence (red) and simultaneously labeled to visualize the hippocampal pathway terminations (green). Scale bar, 250 µm. (*B*) Enlarged site of the gray boxed areas from an upper layer (top panel) and a deep layer (bottom panel) site from A. (*C*, *D*) Two examples of hippocampal axon boutons (black) labeled with DAB that formed synapses on spines that contain D1 receptors (single arrow; D1 receptors were labeled with TMB); panels below show 2 adjacent EM sections for each hippocampal bouton revealing consistent label of D1 receptors in the innervated spines. Double-headed arrow (*C*, left): mitochondrion. Scale bar, 0.5 µm.

et al. 2000; Ghashghaei et al. 2007; Wang et al. 2013; Raper et al. 2017). Lesions of the hippocampus in primates lead to impaired emotional responses and anxiety (Chudasama et al. 2008; Machado and Bachevalier 2008; Chudasama et al. 2009). Moreover, A25 has robust bidirectional connections with the amygdala (Ghashghaei et al. 2007) and heavily innervates the nucleus accumbens in rodents and primates (Haber et al. 1995). The connections of A25 put it in a unique position to regulate emotion and motivation. The direct pathway from hippocampus to A25 thus can play an important role in connecting hippocampal processes with emotion-related processes.

Hippocampal terminations innervated widespread parts of A25, suggesting that they modulate A25 in a dynamic way. As a large structure, the dorsal part of A25 may be important for representing aversive stimuli, whereas the ventral part may encode reward (Monosov and Hikosaka 2012; Wallis et al. 2019). We found that the hippocampus targets robustly the deep layers of posterior A25, and all layers of dorsal A25. The hippocampus thus may influence diverse processes in behavior.

Hippocampal terminations innervated both the upper and deep layers of A25, suggesting a combination of "feedback" and "feedforward" patterns, by analogy with cortical sensory systems (Medalla and Barbas 2006; Barbas 2015; Hilgetag et al. 2016). The feedback component of the projection, which innervates the upper layers of A25, contacts the distal and midapical dendrites of pyramidal neurons and may play a modulatory role (Shao and Burkhalter 1996; Elston 2002; Elston and DeFelipe 2002; Elston 2003). The feedforward component of the hippocampal projection, which innervates the deep layers of posterior A25, may drive neurons that send broad feedback type projections to cortex (Joyce and Barbas 2018), as well as downstream subcortical structures associated with motivational functions and emotional expression (Haber et al. 1995; Chiba et al. 2001; Ghashghaei et al. 2007). Thus, the hippocampal terminations in the upper and deep layers may differentially modulate functional systems in A25 by exciting distinct laminar compartments.

The trend of hippocampal terminations in the upper layers in the anterior to mid-level of A25 and the deep layers in posterior A25 also suggests distinct influence along this ACC region at the cortical level. The bias for a feedback pattern of projection to the upper layers in anterior A25, and feedforward projection to the deep layers of posterior A25 is consistent with the rules of the structural model of connections (reviewed in Barbas 2015; Garcia-Cabezas et al. 2019), since A25 has a comparatively more differentiated layer IV anteriorly than posteriorly. This finding thus extends the application of the structural model for corticocortical connections (Barbas and Rempel-Clower 1997) to the pathway from the subcortical hippocampus to cortical A25.

The Hippocampus has Predominant Excitatory Effects in A25

Nearly 90% of hippocampal terminations in both the upper and deep layers of A25 innervated spines of presumed excitatory neurons. This bias towards excitatory postsynaptic sites is higher than in most pathways studied in monkeys (Bunce and Barbas 2011; Medalla and Barbas 2012; Timbie and Barbas 2014; Wang and Barbas 2018), and comparable with pathways from ACC to olfactory cortices and posterior orbitofrontal cortex (García-Cabezas and Barbas 2014, 2017).

Functional imaging studies in humans have shown that activity in ventro-mPFC and the hippocampus is positively correlated when extinguished stimuli are presented during recall of extinction, and this correlation is impaired in patients with PTSD (Kalisch et al. 2006; Milad et al. 2007; Milad et al. 2009), reviewed in (Milad and Quirk 2012). Moreover, studies in monkeys have shown that hippocampal activation can have anxiolytic effects that are A25 dependent (Zeredo et al. 2019). Similar effects were also found for the hippocampus to mPFC pathway in rodents (Adhikari et al. 2011; Sotres-Bayon et al. 2012), reviewed in (Corcoran and Quirk 2007; Hartley and Phelps 2010). This evidence suggests that the hippocampal pathway carrying contextual and memory-related information may enhance the activity of excitatory neurons in A25, facilitate recall of extinction and thereby boost anxiolytic effects (Strange et al. 2014; Sekeres et al. 2018).

Among the small proportion of hippocampal terminations that innervated inhibitory neurons, we found that most contacted CR neurons. In the upper layers, GABAergic CR neurons are thought to disinhibit pyramidal neurons in the primate cortex (Conde et al. 1994; Gabbott and Bacon 1996a, 1996b; Gabbott et al. 1997; Melchitzky et al. 2005). This pattern may allow hippocampal terminations to increase the gain of a functional subpopulation of pyramidal neurons in the target area, as shown in mice (Pi et al. 2013). On the other hand, in the deep layers CR neurons may innervate and inhibit pyramidal (excitatory) neurons in primate cortex (Gabbott et al. 1997; Meskenaite 1997).

The pattern of innervation of inhibitory postsynaptic sites found here for rhesus monkeys differs from rats, where hippocampal terminations preferentially target PV inhibitory neurons (Gabbott et al. 2002; Tierney et al. 2004; Marek et al. 2018), which exercise strong perisomatic inhibition of nearby pyramidal neurons. This inter-species difference aligns with the differential distribution of PV inhibitory neurons: they are abundant in the IL region of rodents, but sparse in A25 of monkeys (Fig. 8A, D; Kawaguchi and Kubota 1997; Dombrowski et al. 2001; Kawaguchi and Kondo 2002; Garcia-Cabezas et al. 2017).

Dopamine via D1 Receptors may Preferentially Enhance Hippocampal Input to Deep Layers of A25

Our data suggest that the hippocampus has comparable innervation of the upper and deep layers of A25. However, we suggest that the hippocampal terminations in the deep layers of A25 may be more prone to modulation by dopamine, as revealed by a higher density of D1 receptors and a higher proportion of terminations that formed synapses on spines with D1 receptors. These findings are consistent with previous studies in both rats and primates (Lidow et al. 1991; Vincent et al. 1993; Williams and Goldman-Rakic 1993; Carr and Sesack 1996). Given the prominent role of dopamine in learning and motivation, the question arises of how dopamine signaling can affect the hippocampal pathway in A25. Studies in rats have shown that the input from the hippocampus to mPFC is enhanced by increasing dopamine release via VTA stimulation or local infusion of a D1 agonist (Gurden et al. 1999; Gurden et al. 2000). So far no studies have focused on dopamine modulation of the direct hippocampal pathway to A25 in primates. However, a similar effect as in rodents may be expected because activating D1 receptors can facilitate excitatory inputs in primates (Cepeda et al. 1992; Henze et al. 2000). This evidence suggests that the hippocampal inputs to the deep layers are more likely to be enhanced by D1 receptor activation compared with the upper layers.

Dopamine levels in prefrontal regions can vary depending on behavioral, motivational and emotional signals. A variety of events can trigger increases in the firing of VTA dopamine neurons, including those related to reward, reward-prediction error, motivational value, and motivational salience (Kodama et al. 2014; Ellwood et al. 2017; Schultz et al. 1997), reviewed in (Bromberg-Martin et al. 2010; Berke 2018). In addition, a major trigger of elevated mesolimbic dopamine is stress (Arnsten 2000; Lataster et al. 2011; Nagano-Saito et al. 2013) reviewed in (Arnsten et al. 2015). Hippocampal inputs to distinct layers thus may be enhanced differentially by state-dependent activation of D1 receptors (Fig. 10). In healthy individuals, elevated dopamine induced by uncertainty, conflict, or changes in reward contingency may enhance hippocampal inputs in the deep layers of A25 to enable flexible action switching and maintenance (Ellwood et al. 2017). The deep layers are a key source of excitation to the nucleus accumbens, which is critical for motivation and goal-directed action (Haber et al. 1995; Phillips et al. 2003; Gabbott et al. 2005), reviewed in (Berke 2018; Van der Weele et al. 2019).

In states of high stress, elevated dopamine may abnormally potentiate hippocampal terminations in both the upper and deep layers of A25, contributing to over-activation. This, in turn, may trigger abnormally high levels of activity in downstream autonomic structures (Barbas et al. 2003), resulting in the demotivating and anhedonic effects observed in both rodents and primates (Mayberg 1997; Ferenczi et al. 2016; Alexander et al. 2019b). This effect of dopamine is consistent with the general finding that over-activation of mouse mPFC can inhibit behavioral motivation (Ferenczi et al. 2016). In marmosets, over-activation of A25 dampens reward seeking activity (Alexander et al. 2019b). The effect of dopamine on hippocampal terminations in A25 may thus contribute to the emergence of low motivation and anhedonia in major depression. Studies in depressed patients have shown enhancement of functional connectivity between the hippocampus and prefrontal cortex (Seminowicz et al. 2004; Goveas et al. 2011; Lambert et al. 2017), which may arise due to stress-elicited elevation of dopamine (Lataster et al. 2011; Nagano-Saito et al. 2013). In conclusion, different levels of dopamine may differentially modulate hippocampal inputs to the upper and deep layers of A25. Appropriate levels of dopamine may allow A25 to contribute to action initiation via downstream structures, but excessive dopamine may interfere with action and motivation.

The effects of dopamine on A25 may be analogous to the "inverted U" curve associated with dorsolateral prefrontal cortex, where there is an optimal level of dopamine release for normal attention and working memory, outside of which performance declines (Williams and Goldman-Rakic 1995; Arnsten and Goldman-Rakic 1998; Vijayraghavan et al. 2007; Arnsten et al. 2015). Some of these effects may arise due to the reduction in neural firing in dorsolateral prefrontal cortex caused by excessive dopamine (Urban et al. 2002). The precise nature of the effects of dopamine on A25 activity is not yet known, but the evidence reviewed above raises the possibility of an "inverted U" relationship between A25 dopamine and motivation. Consistent with this idea, optogenetic stimulation of VTA projections to mPFC leads to freezing in mice in an aversive situation (Van der Weele et al. 2019). The overabundance of dopamine during stress may have a net excitatory effect on A25 activity via D1 receptors (Seamans and Yang 2004), a hypothesis that can be explored in future studies.

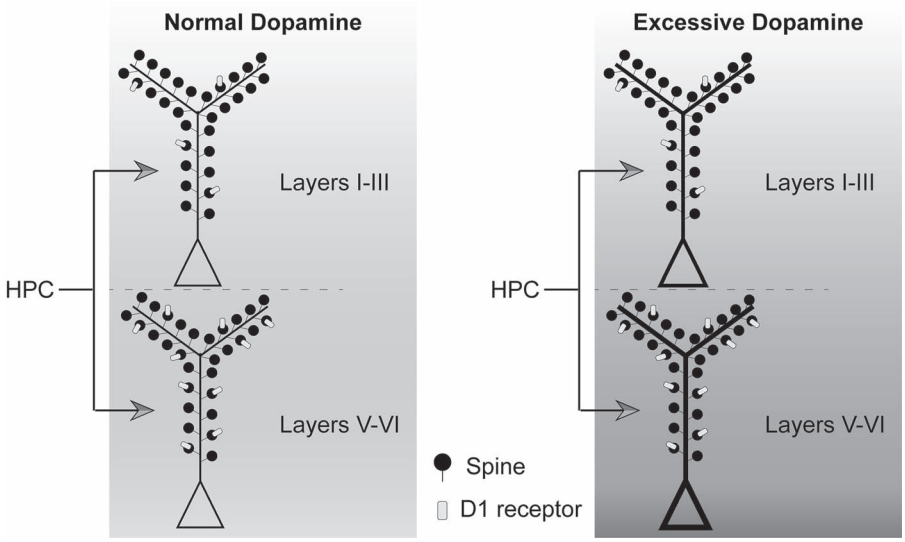

Figure 10. Schematic summary of hippocampal terminations in the upper and deep layers of A25 and relationship to postsynaptic D1 receptors. Hippocampal terminations were comparable in the upper and deep layers of A25 in size and proportion on each type of postsynaptic target. More hippocampal axon boutons formed synapses on spines with D1 receptors (light gray) in the deep layers than in the upper layers, consistent with the distribution of D1 receptors in A25. The background color indicates the effect of dopamine on the pyramidal neuron. Left, Proposed circuit engagement for novelty, uncertainty, and rewards that can elevate dopamine level within the normal range in healthy individuals and enhance information transfer from hippocampus to A25 to modulate goal-directed action via downstream structures. Right, Proposed circuit activation during abnormal states, including uncontrollable stress that excessively increases dopamine level, accompanied by overactivity in A25 and likely demotivating and anhedonic effects that disable goal-directed action, as seen in major depression.

Human studies have shown an inverse functional relationship between dorsolateral prefrontal cortex and A25 in depression (Mayberg et al. 1999; Mayberg 2003; Mayberg et al. 2005). Decreased activity of dorsolateral prefrontal cortex is associated with over-activation of A25 and loss of top-down control during high stress (Mayberg 1997; Arnsten et al. 2012). In view of the sparsity of direct pathways from dorsolateral prefrontal cortex to A25 (Joyce and Barbas 2018), A32 may play the role of intermediary between these cortices, as shown through a synaptic mechanism recently (Joyce et al. 2020). Elevated dopaminergic and hippocampal signaling may therefore act synergistically with reduced inhibitory regulation from A32, leading to excess A25 activity and likely reduction in motivation.

Notes

We thank Drs M. Á. García-Cabezas, B. Zikopoulos, and M. Joyce for helpful discussions and Ifeanyirochukwu N. Onochie for some early data gathering. *Conflict of Interest*: The authors declare no competing financial interests.

Funding

National Institutes of Health/National Institute of Mental Health (grants R01-MH-057414 and R01-MH-117785).

References

Adhikari A, Topiwala MA, Gordon JA. 2011. Single units in the medial prefrontal cortex with anxiety-related firing patterns are preferentially influenced by ventral hippocampal activity. *Neuron*. 71:898–910.

Admon R, Lubin G, Stern O, Rosenberg K, Sela L, Ben-Ami H, Hendler T. 2009. Human vulnerability to stress depends on amygdala's predisposition and hippocampal plasticity. *Proc Natl Acad Sci USA*. 106:14120–14125.

Aggleton JP, Wright NF, Rosene DL, Saunders RC. 2015. Complementary patterns of direct amygdala and hippocampal projections to the macaque prefrontal cortex. *Cereb Cortex*. 25:4351–4373.

Alexander L, Clarke HF, Roberts AC. 2019a. A focus on the functions of area 25. *Brain Sci*. 9:1–33.

Alexander L, Gaskin PLR, Sawiak SJ, Fryer TD, Hong YT, Cockcroft GJ, Clarke HF, Roberts AC. 2019b. Fractionating blunted reward processing characteristic of anhedonia by overactivating primate subgenual anterior cingulate cortex. *Neuron*. 101:307–320.

Amaral D, Lavenex P. 2006. Hippocampal neuroanatomy. In: Andersen P, Morris R, Amaral D, Bliss T, O'Keefe J, editors. *The hipppocampus book*. Oxford, England: Oxford University Press.

Amaral DG. 1985. Amygdalohippocampal and amygdalocortical projections in the primate brain. In: Schwarcz R, Ben-Ari Y, editors. *Excitatory amino acids and epilepsy*. Advances in experimental medicine and biology. Vol 203. New York: Plenum Press, pp. 3–17.

Arnsten AF. 2000. Stress impairs prefrontal cortical function in rats and monkeys: role of dopamine D1 and norepinephrine alpha-1 receptor mechanisms. *Prog Brain Res*. 126:183–192.

Arnsten AF, Goldman-Rakic PS. 1998. Noise stress impairs prefrontal cortical cognitive function in monkeys: evidence for a hyperdopaminergic mechanism. *Arch Gen Psychiatry*. 55:362–368.

Arnsten AF, Wang MJ, Paspalas CD. 2012. Neuromodulation of thought: flexibilities and vulnerabilities in prefrontal cortical network synapses. *Neuron*. 76:223–239.

Arnsten AF, Wang M, Paspalas CD. 2015. Dopamine's actions in primate prefrontal cortex: challenges for treating cognitive disorders. *Pharmacol Rev*. 67:681–696.

Bachevalier J. 2019. Nonhuman primate models of hippocampal development and dysfunction. *Proc Natl Acad Sci USA*. 116:26210–26216.

Bakst I, Amaral DG. 1984. The distribution of acetylcholinesterase in the hippocampal formation of the monkey. *J Comp Neurol*. 225:344–371.

Barbas H. 2015. General cortical and special prefrontal connections: principles from structure to function. *Annu Rev Neurosci*. 38:269–289.

Barbas H, Pandya DN. 1989. Architecture and intrinsic connections of the prefrontal cortex in the rhesus monkey. *J Comp Neurol*. 286:353–375.

Barbas H, Blatt GJ. 1995. Topographically specific hippocampal projections target functionally distinct prefrontal areas in the rhesus monkey. *Hippocampus*. 5:511–533.

Barbas H, Rempel-Clower N. 1997. Cortical structure predicts the pattern of corticocortical connections. *Cereb Cortex*. 7:635–646.

Barbas H, Saha S, Rempel-Clower N, Ghashghaei T. 2003. Serial pathways from primate prefrontal cortex to autonomic areas may influence emotional expression. *BMC Neurosci*. 4:25.

Barbas H, Wang J, Joyce MKP, García-Cabezas MA. 2018. Pathway mechanism for excitatory and inhibitory control in working memory. *J Neurophysiol*. 120:2659–2678.

Berke JD. 2018. What does dopamine mean? *Nat Neurosci*. 21:787–793.

Bourne JN, Harris KM. 2008. Balancing structure and function at hippocampal dendritic spines. *Annu Rev Neurosci*. 31:47–67.

Bromberg-Martin ES, Matsumoto M, Hikosaka O. 2010. Dopamine in motivational control: rewarding, aversive, and alerting. *Neuron*. 68:815–834.

Bunce JG, Barbas H. 2011. Prefrontal pathways target excitatory and inhibitory systems in memory-related medial temporal cortices. *Neuroimage*. 55:1461–1474.

Carr DB, Sesack SR. 1996. Hippocampal afferents to the rat prefrontal cortex: synaptic targets and relation to dopamine terminals. *J Comp Neurol*. 369:1–15.

Cepeda C, Radisavljevic Z, Peacock W, Levine MS, Buchwald NA. 1992. Differential modulation by dopamine of responses evoked by excitatory amino acids in human cortex. *Synapse*. 11:330–341.

Chiba T, Kayahara T, Nakano K. 2001. Efferent projections of infralimbic and prelimbic areas of the medial prefrontal cortex in the Japanese monkey, *Macaca fuscata*. *Brain Res*. 888:83–101.

Chudasama Y, Wright KS, Murray EA. 2008. Hippocampal lesions in rhesus monkeys disrupt emotional responses but not reinforcer devaluation effects. *Biol Psychiatry*. 63:1084–1091.

Chudasama Y, Izquierdo A, Murray EA. 2009. Distinct contributions of the amygdala and hippocampus to fear expression. *Eur J Neurosci*. 30:2327–2337.

Conde F, Lund JS, Jacobowitz DM, Baimbridge KG, Lewis DA. 1994. Local circuit neurons immunoreactive for calretinin, calbindin D- 28k or parvalbumin in monkey prefrontal cortex: distribution and morphology. *J Comp Neurol*. 341:95–116.

Corcoran KA, Quirk GJ. 2007. Recalling safety: cooperative functions of the ventromedial prefrontal cortex and the hippocampus in extinction. *CNS Spectr*. 12:200–206.

DeFelipe J. 1997. Types of neurons, synaptic connections and chemical characteristics of cells immunoreactive for calbindin-D28K, parvalbumin and calretinin in the neocortex. *J Chem Neuroanat*. 14:1–19.

Desmond NL, Weinberg RJ. 1998. Enhanced expression of AMPA receptor protein at perforated axospinous synapses. *Neuroreport*. 9:857–860.

Dickie EW, Brunet A, Akerib V, Armony JL. 2011. Neural correlates of recovery from post-traumatic stress disorder: a longitudinal fMRI investigation of memory encoding. *Neuropsychologia*. 49:1771–1778.

Dombrowski SM, Hilgetag CC, Barbas H. 2001. Quantitative architecture distinguishes prefrontal cortical systems in the rhesus monkey. *Cereb Cortex*. 11:975–988.

Eichenbaum H. 2017. Prefrontal-hippocampal interactions in episodic memory. *Nat Rev Neurosci*. 18:547–558.

Ellwood IT, Patel T, Wadia V, Lee AT, Liptak AT, Bender KJ, Sohal VS. 2017. Tonic or phasic stimulation of dopaminergic projections to prefrontal cortex causes mice to maintain or deviate from previously learned Behavioral strategies. *J Neurosci*. 37:8315–8329.

Elston GN. 2002. Cortical heterogeneity: implications for visual processing and polysensory integration. *J Neurocytol*. 31:317–335.

Elston GN. 2003. Cortex, cognition and the cell: new insights into the pyramidal neuron and prefrontal function. *Cereb Cortex*. 13:1124–1138.

Elston GN, DeFelipe J. 2002. Spine distribution in cortical pyramidal cells: a common organizational principle across species. *Prog Brain Res*. 136:109–133.

Ferenczi EA, Zalocusky KA, Liston C, Grosenick L, Warden MR, Amatya D, Katovich K, Mehta H, Patenaude B, Ramakrishnan C *et al*. 2016. Prefrontal cortical regulation of brainwide circuit dynamics and reward-related behavior. *Science*. 351:aac9698.

Fiala JC. 2005. Reconstruct: a free editor for serial section microscopy. *J Microsc*. 218:52–61.

Gabbott P, Headlam A, Busby S. 2002. Morphological evidence that CA1 hippocampal afferents monosynaptically innervate PV-containing neurons and NADPH-diaphorase reactive cells in the medial prefrontal cortex (areas 25/32) of the rat. *Brain Res*. 946:314–322.

Gabbott PL, Bacon SJ. 1996a. Local circuit neurons in the medial prefrontal cortex (areas 24a,b,c, 25 and 32) in the monkey: I. cell morphology and morphometrics. *J Comp Neurol*. 364:567–608.

Gabbott PL, Bacon SJ. 1996b. Local circuit neurons in the medial prefrontal cortex (areas 24a,b,c, 25 and 32) in the monkey: II. Quantitative areal and laminar distributions. *J Comp Neurol*. 364:609–636.

Gabbott PL, Warner TA, Jays PR, Salway P, Busby SJ. 2005. Prefrontal cortex in the rat: projections to subcortical autonomic, motor, and limbic centers. *J Comp Neurol*. 492:145–177.

Gabbott PLA, Jays PRL, Bacon SJ. 1997. Calretinin neurons in human medial prefrontal cortex (areas 24a,b,c, 32′, and 25). *J Comp Neurol*. 381:389–410.

Gage FH, Thompson RG. 1980. Differential distribution of norepinephrine and serotonin along the dorsal-ventral axis of the hippocampal formation. *Brain Res Bull*. 5:771–773.

Garcia-Cabezas MA, Zikopoulos B, Barbas H. 2019. The structural model: a theory linking connections, plasticity, pathology, development and evolution of the cerebral cortex. *Brain Struct Funct*. 224:985–1008.

Garcia-Cabezas MA, Joyce MP, John Y, Zikopoulos B, Barbas H. 2017. Mirror trends of plasticity and stability indicators in primate prefrontal cortex. *Eur J Neurosci*. 46: 2392–2405.

García-Cabezas MA, Barbas H. 2014. A direct anterior cingulate pathway to the primate primary olfactory cortex may control attention to olfaction. *Brain Struct Funct*. 219:1735–1754.

García-Cabezas MA, Barbas H. 2017. Anterior cingulate pathways may affect emotions through orbitofrontal cortex. *Cereb Cortex*. 27:4891–4910.

Geinisman Y. 1993. Perforated axospinous synapses with multiple, completely partitioned transmission zones: probable structural intermediates in synaptic plasticity. *Hippocampus*. 3:417–433.

Germuska M, Saha S, Fiala J, Barbas H. 2006. Synaptic distinction of laminar-specific prefrontal-temporal pathways in primates. *Cereb Cortex*. 16:865–875.

Ghashghaei HT, Hilgetag CC, Barbas H. 2007. Sequence of information processing for emotions based on the anatomic dialogue between prefrontal cortex and amygdala. *Neuroimage*. 34:905–923.

Godsil BP, Kiss JP, Spedding M, Jay TM. 2013. The hippocampal-prefrontal pathway: the weak link in psychiatric disorders? *Eur Neuropsychopharmacol*. 23:1165–1181.

Goveas J, Xie C, Wu Z, Douglas Ward B, Li W, Franczak MB, Jones JL, Antuono PG, Yang Z, Li SJ. 2011. Neural correlates of the interactive relationship between memory deficits and depressive symptoms in nondemented elderly: resting fMRI study. *Behav Brain Res*. 219:205–212.

Gurden H, Tassin JP, Jay TM. 1999. Integrity of the mesocortical dopaminergic system is necessary for complete expression of in vivo hippocampal-prefrontal cortex long-term potentiation. *Neuroscience*. 94:1019–1027.

Gurden H, Takita M, Jay TM. 2000. Essential role of D1 but not D2 receptors in the NMDA receptor-dependent long-term potentiation at hippocampal-prefrontal cortex synapses in vivo. *J Neurosci*. 20:RC106.

Haber SN, Kunishio K, Mizobuchi M, Lynd-Balta E. 1995. The orbital and medial prefrontal circuit through the primate basal ganglia. *J Neurosci*. 15:4851–4867.

Hartley CA, Phelps EA. 2010. Changing fear: the neurocircuitry of emotion regulation. *Neuropsychopharmacology*. 35:136–146.

Heilbronner SR, Rodriguez-Romaguera J, Quirk GJ, Groenewegen HJ, Haber SN. 2016. Circuit-based corticostriatal homologies between rat and primate. *Biol Psychiatry*. 80:509–521.

Henze DA, Gonzalez-Burgos GR, Urban NN, Lewis DA, Barrionuevo G. 2000. Dopamine increases excitability of pyramidal neurons in primate prefrontal cortex. *J Neurophysiol*. 84:2799–2809.

Hilgetag CC, Medalla M, Beul S, Barbas H. 2016. The primate connectome in context: principles of connections of the cortical visual system. *Neuroimage*. 134:685–702.

Insausti R, Munoz M. 2001. Cortical projections of the non-entorhinal hippocampal formation in the cynomolgus monkey (*Macaca fascicularis*). *Eur J Neurosci*. 14:435–451.

Insausti R, Marcos P, Mohedano-Moriano A, Córcoles-Parada M, Artacho-Pérula E, Ubero-Martínez M, Muñoz-López M. 2017. The nonhuman primate hippocampus: neuroanatomy and patterns of cortical connectivity. In: Hannula H, Duff M, editors. *The hippocampus from cells to systems*. Cham: Springer.

Jacobson L, Sapolsky R. 1991. The role of the hippocampus in feedback regulation of the hypothalamic-pituitary-adrenocortical axis. *Endocr Rev*. 12:118–134.

Jay TM, Witter MP. 1991. Distribution of hippocampal CA1 and subicular efferents in the prefrontal cortex of the rat studied by means of anterograde transport of *Phaseolus vulgaris*-leucoagglutinin. *J Comp Neurol*. 313:574–586.

Jay TM, Thierry AM, Wiklund L, Glowinski J. 1992. Excitatory amino acid pathway from the hippocampus to the prefrontal cortex. Contribution of AMPA receptors in hippocampo-prefrontal cortex transmission. *Eur J Neurosci*. 4:1285–1295.

Joyce MKP, Garcia-Cabezas MA, John Y, Barbas H. 2020. Serial prefrontal pathways are positioned to balance cognition and emotion in primates. *J Neurosci*. 40:8306–8328.

Joyce MP, Barbas H. 2018. Cortical connections position primate area 25 as a keystone for interoception, emotion, and memory. *J Neurosci*. 38:1677–1698.

Kalisch R, Korenfeld E, Stephan KE, Weiskopf N, Seymour B, Dolan RJ. 2006. Context-dependent human extinction memory is mediated by a ventromedial prefrontal and hippocampal network. *J Neurosci*. 26:9503–9511.

Kawaguchi Y, Kubota Y. 1997. GABAergic cell subtypes and their synaptic connections in rat frontal cortex. *Cereb Cortex*. 7:476–486.

Kawaguchi Y, Kondo S. 2002. Parvalbumin, somatostatin and cholecystokinin as chemical markers for specific GABAergic interneuron types in the rat frontal cortex. *J Neurocytol*. 31:277–287.

Koch K, Schultz CC, Wagner G, Schachtzabel C, Reichenbach JR, Sauer H, Schlosser RG. 2013. Disrupted white matter connectivity is associated with reduced cortical thickness in the cingulate cortex in schizophrenia. *Cortex*. 49:722–729.

Kodama T, Hikosaka K, Honda Y, Kojima T, Watanabe M. 2014. Higher dopamine release induced by less rather than more preferred reward during a working memory task in the primate prefrontal cortex. *Behav Brain Res*. 266:104–107.

Kondo H, Tanaka K, Hashikawa T, Jones EG. 1999. Neurochemical gradients along monkey sensory cortical pathways: calbindin-immunoreactive pyramidal neurons in layers II and III. *Eur J Neurosci*. 11:4197–4203.

Lambert HK, Sheridan MA, Sambrook KA, Rosen ML, Askren MK, McLaughlin KA. 2017. Hippocampal contribution to context encoding across development is disrupted following early-life adversity. *J Neurosci*. 37:1925–1934.

Lataster J, Collip D, Ceccarini J, Haas D, Booij L, van Os J, Pruessner J, Van Laere K, Myin-Germeys I. 2011. Psychosocial stress is associated with in vivo dopamine release in human ventromedial prefrontal cortex: a positron emission tomography study using [(18)F]fallypride. *Neuroimage*. 58:1081–1089.

Lidow MS, Goldman-Rakic PS, Gallager DW, Rakic P. 1991. Distribution of dopaminergic receptors in the primate cerebral cortex: quantitative autoradiographic analysis using [3H]raclopride, [3H]spiperone and [3H]SCH23390. *Neuroscience*. 40:657–671.

Liu X, Carter AG. 2018. Ventral hippocampal inputs preferentially drive corticocortical neurons in the infralimbic prefrontal cortex. *J Neurosci*. 38:7351–7363.

Machado CJ, Bachevalier J. 2008. Behavioral and hormonal reactivity to threat: effects of selective amygdala, hippocampal or orbital frontal lesions in monkeys. *Psychoneuroendocrinology*. 33:926–941.

Mackey S, Petrides M. 2014. Architecture and morphology of the human ventromedial prefrontal cortex. *Eur J Neurosci*. 40:2777–2796.

Marek R, Jin J, Goode TD, Giustino TF, Wang Q, Acca GM, Holehonnur R, Ploski JE, Fitzgerald PJ, Lynagh T *et al*. 2018. Hippocampus-driven feed-forward inhibition of the prefrontal cortex mediates relapse of extinguished fear. *Nat Neurosci*. 21:384–392.

Mayberg HS. 1997. Limbic-cortical dysregulation: a proposed model of depression. *J Neuropsychiatry Clin Neurosci*. 9:471–481.

Mayberg HS. 2003. Modulating dysfunctional limbic-cortical circuits in depression: towards development of brain-based algorithms for diagnosis and optimised treatment. *Br Med Bull*. 65:193–207.

Mayberg HS, Lozano AM, Voon V, McNeely HE, Seminowicz D, Hamani C, Schwalb JM, Kennedy SH. 2005. Deep brain stimulation for treatment-resistant depression. *Neuron*. 45: 651–660.

Mayberg HS, Liotti M, Brannan SK, McGinnis S, Mahurin RK, Jerabek PA, Silva JA, Tekell JL, Martin CC, Lancaster JL *et al.* 1999. Reciprocal limbic-cortical function and negative mood: converging PET findings in depression and normal sadness. *Am J Psychiatry*. 156:675–682.

Medalla M, Barbas H. 2006. Diversity of laminar connections linking periarcuate and lateral intraparietal areas depends on cortical structure. *Eur J Neurosci*. 23:161–179.

Medalla M, Barbas H. 2009. Synapses with inhibitory neurons differentiate anterior cingulate from dorsolateral prefrontal pathways associated with cognitive control. *Neuron*. 61:609–620.

Medalla M, Barbas H. 2012. The anterior cingulate cortex may enhance inhibition of lateral prefrontal cortex via m2 cholinergic receptors at dual synaptic sites. *J Neurosci*. 32:15611–15625.

Medalla M, Luebke JI. 2015. Diversity of glutamatergic synaptic strength in lateral prefrontal versus primary visual cortices in the rhesus monkey. *J Neurosci*. 35:112–127.

Medalla M, Lera P, Feinberg M, Barbas H. 2007. Specificity in inhibitory systems associated with prefrontal pathways to temporal cortex in primates. *Cereb Cortex*. 17(Suppl 1): i136–i150.

Melchitzky DS, Lewis DA. 2008. Dendritic-targeting GABA neurons in monkey prefrontal cortex: comparison of somatostatin- and calretinin-immunoreactive axon terminals. *Synapse*. 62:456–465.

Melchitzky DS, Eggan SM, Lewis DA. 2005. Synaptic targets of calretinin-containing axon terminals in macaque monkey prefrontal cortex. *Neuroscience*. 130:185–195.

Meskenaite V. 1997. Calretinin-immunoreactive local circuit neurons in area 17 of the cynomolgus monkey, *Macaca fascicularis*. *J Comp Neurol*. 379:113–132.

Milad MR, Quirk GJ. 2012. Fear extinction as a model for translational neuroscience: ten years of progress. *Annu Rev Psychol*. 63:129–151.

Milad MR, Wright CI, Orr SP, Pitman RK, Quirk GJ, Rauch SL. 2007. Recall of fear extinction in humans activates the ventromedial prefrontal cortex and hippocampus in concert. *Biol Psychiatry*. 62:446–454.

Milad MR, Pitman RK, Ellis CB, Gold AL, Shin LM, Lasko NB, Zeidan MA, Handwerger K, Orr SP, Rauch SL. 2009. Neurobiological basis of failure to recall extinction memory in posttraumatic stress disorder. *Biol Psychiatry*. 66: 1075–1082.

Monosov IE, Hikosaka O. 2012. Regionally distinct processing of rewards and punishments by the primate ventromedial prefrontal cortex. *J Neurosci*. 32:10318–10330.

Munoz M, Insausti R. 2005. Cortical efferents of the entorhinal cortex and the adjacent parahippocampal region in the monkey (*Macaca fascicularis*). *Eur J Neurosci*. 22:1368–1388.

Nagano-Saito A, Dagher A, Booij L, Gravel P, Welfeld K, Casey KF, Leyton M, Benkelfat C. 2013. Stress-induced dopamine release in human medial prefrontal cortex–18F-fallypride/PET study in healthy volunteers. *Synapse*. 67: 821–830.

Nava N, Chen F, Wegener G, Popoli M, Nyengaard JR. 2014. A new efficient method for synaptic vesicle quantification reveals differences between medial prefrontal cortex perforated and nonperforated synapses. *J Comp Neurol*. 522:284–297.

Palomero-Gallagher N, Vogt BA, Schleicher A, Mayberg HS, Zilles K. 2009. Receptor architecture of human cingulate cortex: evaluation of the four-region neurobiological model. *Hum Brain Mapp*. 30:2336–2355.

Parent MA, Wang L, Su J, Netoff T, Yuan LL. 2010. Identification of the hippocampal input to medial prefrontal cortex in vitro. *Cereb Cortex*. 20:393–403.

Peters A, Palay SL, Webster HD. 1991. *The fine structure of the nervous system. Neurons and their supporting cells*. 3rd ed. New York (NY): Oxford University Press.

Phillips PE, Stuber GD, Heien ML, Wightman RM, Carelli RM. 2003. Subsecond dopamine release promotes cocaine seeking. *Nature*. 422:614–618.

Pi HJ, Hangya B, Kvitsiani D, Sanders JI, Huang ZJ, Kepecs A. 2013. Cortical interneurons that specialize in disinhibitory control. *Nature*. 503:521–524.

Pitkanen A, Pikkarainen M, Nurminen N, Ylinen A. 2000. Reciprocal connections between the amygdala and the hippocampal formation, perirhinal cortex, and postrhinal cortex in rat. A review. *Ann N Y Acad Sci*. 911:369–391.

Qiu A, Tuan TA, Woon PS, Abdul-Rahman MF, Graham S, Sim K. 2010. Hippocampal-cortical structural connectivity disruptions in schizophrenia: an integrated perspective from hippocampal shape, cortical thickness, and integrity of white matter bundles. *Neuroimage*. 52:1181–1189.

Raper J, Wilson M, Sanchez M, Payne C, Bachevalier J. 2017. Increased anxiety-like behaviors, but blunted cortisol stress response after neonatal hippocampal lesions in monkeys. *Psychoneuroendocrinology*. 76:57–66.

Rocco BR, Sweet RA, Lewis DA, Fish KN. 2016. GABA-synthesizing enzymes in calbindin and calretinin neurons in monkey prefrontal cortex. *Cereb Cortex*. 26:2191–2204.

Rosene DL, Van Hoesen GW. 1987. The hippocampal formation of the primate brain. A review of some comparative aspects of cytoarchitecture and connections. In: Jones EG, Peters A, editors. *Cerebral cortex*. Vol 6. New York: Plenum Publishing Corporation, pp. 345–455.

Saunders RC, Rosene DL, Van Hoesen GW. 1988. Comparison of the efferents of the amygdala and the hippocampal formation in the rhesus monkey: II. Reciprocal and non- reciprocal connections. *J Comp Neurol*. 271:185–207.

Schultz W, Dayan P, Montague PR. 1997. A neural substrate of prediction and reward. *Science*. 275:1593–1599.

Seamans JK, Yang CR. 2004. The principal features and mechanisms of dopamine modulation in the prefrontal cortex. *Prog Neurobiol*. 74:1–58.

Sekeres MJ, Winocur G, Moscovitch M. 2018. The hippocampus and related neocortical structures in memory transformation. *Neurosci Lett*. 680:39–53.

Seminowicz DA, Mayberg HS, McIntosh AR, Goldapple K, Kennedy S, Segal Z, Rafi-Tari S. 2004. Limbic-frontal circuitry in major depression: a path modeling metanalysis. *Neuroimage*. 22:409–418.

Shao Z, Burkhalter A. 1996. Different balance of excitation and inhibition in forward and feedback circuits of rat visual cortex. *J Neurosci*. 16:7353–7365.

Siegel A, Tassoni JP. 1971. Differential efferent projections from the ventral and dorsal hippocampus of the cat. *Brain Behav Evol*. 4:185–200.

Smiley JF, Levey AI, Ciliax BJ, Goldman-Rakic PS. 1994. D1 dopamine receptor immunoreactivity in human and monkey cerebral cortex: predominant and extrasynaptic localization in dendritic spines. *Proc Natl Acad Sci USA*. 91:5720–5724.

Sotres-Bayon F, Sierra-Mercado D, Pardilla-Delgado E, Quirk GJ. 2012. Gating of fear in prelimbic cortex by hippocampal and amygdala inputs. *Neuron*. 76:804–812.

Stevens CF. 2004. Presynaptic function. *Curr Opin Neurobiol*. 14:341–345.

Strange BA, Witter MP, Lein ES, Moser EI. 2014. Functional organization of the hippocampal longitudinal axis. *Nat Rev Neurosci*. 15:655–669.

Thierry AM, Gioanni Y, Degenetais E, Glowinski J. 2000. Hippocampo-prefrontal cortex pathway: anatomical and electrophysiological characteristics. *Hippocampus*. 10: 411–419.

Thomson AM. 2000. Molecular frequency filters at central synapses. *ProgNeurobiol*. 62:159–196.

Tierney PL, Degenetais E, Thierry AM, Glowinski J, Gioanni Y. 2004. Influence of the hippocampus on interneurons of the rat prefrontal cortex. *Eur J Neurosci*. 20:514–524.

Timbie C, Barbas H. 2014. Specialized pathways from the primate amygdala to posterior orbitofrontal cortex. *J Neurosci*. 34:8106–8118.

Urban NN, Gonzalez-Burgos G, Henze DA, Lewis DA, Barrionuevo G. 2002. Selective reduction by dopamine of excitatory synaptic inputs to pyramidal neurons in primate prefrontal cortex. *J Physiol*. 539:707–712.

Van der Weele CMV, Siciliano CA, Tye KM. 2019. Dopamine tunes prefrontal outputs to orchestrate aversive processing. *Brain Res*. 1713:16–31.

Verwer RW, Meijer RJ, Van Uum HF, Witter MP. 1997. Collateral projections from the rat hippocampal formation to the lateral and medial prefrontal cortex. *Hippocampus*. 7:397–402.

Vijayraghavan S, Wang M, Birnbaum SG, Williams GV, Arnsten AF. 2007. Inverted-U dopamine D1 receptor actions on prefrontal neurons engaged in working memory. *Nat Neurosci*. 10:376–384.

Vincent SL, Khan Y, Benes FM. 1993. Cellular distribution of dopamine D1 and D2 receptors in rat medial prefrontal cortex. *J Neurosci*. 13:2551–2564.

Vogt BA, Hof PR, Zilles K, Vogt LJ, Herold C, Palomero-Gallagher N. 2013. Cingulate area 32 homologies in mouse, rat, macaque and human: cytoarchitecture and receptor architecture. *J Comp Neurol*. 521:4189–4204.

Wallis CU, Cockcroft GJ, Cardinal RN, Roberts AC, Clarke HF. 2019. Hippocampal interaction with area 25, but not area 32. *Cereb Cortex*. 29:4818–4830.

Wang J, Barbas H. 2018. Specificity of primate amygdalar pathways to hippocampus. *J Neurosci*. 38:10019–10041.

Wang ME, Fraize NP, Yin L, Yuan RK, Petsagourakis D, Wann EG, Muzzio IA. 2013. Differential roles of the dorsal and ventral hippocampus in predator odor contextual fear conditioning. *Hippocampus*. 23:451–466.

Wang XJ, Tegner J, Constantinidis C, Goldman-Rakic PS. 2004. Division of labor among distinct subtypes of inhibitory neurons in a cortical microcircuit of working memory. *Proc Natl Acad Sci USA*. 101:1368–1373.

West M. 2012. Introduction to stereology. In: *Basic stereology for biologists and neuroscientists*. Long Island, New York: Cold Spring Harbor Laboratory Press, pp. 843–851.

Williams GV, Goldman-Rakic PS. 1995. Modulation of memory fields by dopamine D1 receptors in prefrontal cortex. *Nature*. 376:572–575.

Williams SM, Goldman-Rakic PS. 1993. Characterization of the dopaminergic innervation of the primate frontal-cortex using a dopamine-specific antibody. *Cereb Cortex*. 3: 199–222.

Zeredo JL, Quah SKL, Wallis CU, Alexander L, Cockcroft GJ, Santangelo AM, Xia J, Shiba Y, Dalley JW, Cardinal RN *et al*. 2019. Glutamate within the marmoset anterior hippocampus interacts with area 25 to regulate the behavioral and cardiovascular correlates of high-trait anxiety. *J Neurosci*. 39:3094–3107.